Effects of LHRF on Toroidal Rotation in Alcator C-Mod Plasmas

J.E. Rice, Y.A. Podpaly, M.L. Reinke, C. Gao, S. Shiraiwa, J.L. Terry, C. Theiler, G.M. Wallace, P.T. Bonoli, D. Brunner, R.M. Churchill, I. Cziegler[‡], L. Delgado-Aparicio[þ], P.H. Diamond[‡], I.C. Faust, N.J. Fisch[þ], R.S. Granetz, M.J. Greenwald, A.E. Hubbard, J.W.Hughes, I.H. Hutchinson, J.H. Irby, J. Lee, Y. Lin, E.S. Marmar, R. Mumgaard, R.R. Parker, S.D. Scott[þ], J.R. Walk, S.M. Wolfe and S.J. Wukitch

PSFC, MIT, Cambridge, Massachusetts 02139, USA

[‡]*CMTFO, UCSD, San Diego, California 92903, USA*

[þ]*PPPL, Princeton, New Jersey 08543, USA*

Abstract

Application of lower hybrid RF (LHRF) waves can induce both co- and counter-current directed changes in toroidal rotation in Alcator C-Mod plasmas, depending on the target plasma current, electron density, confinement regime and magnetic shear. For Ohmic L-mode discharges with good core LH wave absorption, and significant current drive, the interior (r/a$<$0.5) rotation increments (on a time scale of order the current relaxation time) in the counter-current direction if $n_e(10^{20}/m^3) > q_{95}/11.5$, and in the co-current direction if $n_e(10^{20}/m^3) < q_{95}/11.5$. All discharges with co-current rotation changes have $q_0 > 1$, indicating a good correlation with driven current fraction, unifying the results observed on various tokamaks. For high density ($n_e \geq 1.2\times10^{20}/m^3$) L-mode target discharges, where core LH wave absorption is low, the rotation change is in the co-current direction, but evolves on a shorter momentum transport time scale, and is seen across the entire spatial profile. For H-mode target plasmas, both co- and counter-current direction increments have been observed with LHRF. The H-mode co-rotation is correlated with the pedestal temperature gradient, which itself is enhanced by the LH waves absorbed in the plasma periphery. The H-mode counter- rotation increment, a flattening of the peaked velocity profile in the core, is consistent with a reduction in the momentum pinch correlated with a steepening of the core density profile. Most of these rotation changes must be due to indirect transport effects of LH waves on various parameters, which modify the momentum flux.

I. Introduction

The benefits of rotation and flow shear for tokamak performance are well known. Toroidal rotation is often provided externally through neutral beam injection, but in future devices, neutral beam torque will be low, and other methods for rotation drive may be necessary. One possiblility is to take advantage of self-generated flow in enhanced confinement regimes [1], but this process relies on plasma performance, which makes for a complicated control knob. Another approach is to utilize radio frequency waves: ion cyclotron, electron cyclotron and lower hybrid. Through asymmetric launching with respect to the toroidal direction, all of these waves have been used to generate toroidal current, for which the current drive mechanisms are well documented [2], but the accompanying changes in the toroidal rotation are not well understood. Ion cyclotron range of frequencies (ICRF) mode conversion flow drive has been demonstrated [3, 4, 5, 6], but the details of the velocity generation process are still unclear. Regarding rotation in ICRF minority heated [7, 8] and ECH [9, 10, 11] discharges, the direct momentum input is expected to be low, and the observed rotation is probably generated intrinsically, through modification of the temperature/pressure profiles. Toroidal rotation changes due to lower hybrid (LH) waves have also been observed [12, 13, 14, 15, 16, 8, 17, 18], with co-current increments seen in JT-60U, Tore Supra, JET, EAST and C-Mod, and counter-current modifications in C-Mod. In plasmas with good core absorption of LH waves, the mechanism for rotation drive is uncertain. Candidates include direct momentum input from the waves [19] (calculated to be low [8]), electron orbit loss [12, 14], trapped electron pinch effects [20], resonant electron radial drift [21, 22], and less direct causes such as the turbulent equipartition pinch [17] or modification of the q profile. A challenge of these accounts is to explain the direction of the change in rotation. The main goal of this paper is to document the rotation changes in C-Mod lower hybrid current drive (LHCD) plasmas, and to understand what determines the rotation increment direction. Also of interest are the rotation drive mechanisms in plasmas without core accessibility of the LH waves, or with poor core absorption. In these cases the source of the rotation is due to alteration of edge plasma conditions, which then leads to core rotation changes following momentum transport [16, 23].

This detailed study of rotation in LHRF plasmas has been performed on the Alcator C-Mod tokamak [24] (major radius R = 0.67 m, typical minor radius of 0.21 m). Operation was in both forward and reversed magnetic field/plasma current, and in the upper single null (USN) and lower single null (LSN) configurations, with deuterium working gas. Line averaged electron densities were in the range from 0.25 to $3.5\times10^{20}/\mathrm{m}^3$, on axis magnetic field between 3.7 and 6.9 T and with plasma currents between 0.3 and 1.1 MA ($10 \geq \mathrm{q}_{95} \geq 3.2$). All target plasmas were sawtoothing before application of LHCD power and discharges with other significant MHD activity have been excluded. Electron densities were determined from a two color interferometer, fast electron temperature evolution using electron cyclotron emission and $\mathrm{Z}_{\mathrm{eff}}$ from visible *bremsstrahlung* [25]. Electron density and temperature profiles were provided by Thomson scattering [25]. Magnetic flux surfaces were generated using EFIT [26] and current density profiles were also calculated from EFIT, where possible constrained by MSE measurements [25, 27, 28]. Density fluctuations in the periphery

were monitored using gas puff imaging [25]. Edge velocity and ion temperature profiles were determined from charge exchange recombination spectroscopy of boron ions [25]. Core toroidal rotation and ion temperature profiles were measured with a high resolution imaging x-ray spectrometer system [29, 30], viewing H- and He-like argon. Unless otherwise noted, toroidal rotation velocities are chord averaged. The velocity calibration was achieved by running locked mode discharges, which are presumed to have zero rotation velocity over the whole profile. Throughout this paper, '$+$' velocity indicates co-current directed rotation, while '$-$' indicates counter-current.

LH waves were introduced from a launcher which consists of 60 waveguides capable of delivering up to 1.2 MW of power at 4.6 GHz, with parallel index of refraction, $n_{||}$, between 1.5 and 4 [31], and with wave momentum input in the counter-current direction. These parameters are favorable for toroidal electric current driven by lower hybrid waves, where the rf-driven current is generated efficiently in the co-current direction [32]. Recent results from C-Mod LHCD experiments may be found in [33, 34, 35, 36, 37]. H-mode is accessed with up to 5 MW of ICRF power, usually by H minority heating in D plasmas [31] at 5.4 T.

An outline of the paper follows. In section II, velocity changes due to LHCD in low density Ohmic L-mode target plasmas (with good core wave absorption) are presented, including spatial rotation profiles, in adddition to scalings with plasma current, electron density and magnetic configuration. Velocity increments in both directions have been observed. A comparison of these results is made with Ohmic rotation reversals in section III. Rotation behavior in higher density L-mode plasmas, with poor core LH wave absorption, is shown in section IV. Corresponding results to those presented in section II are described in section V for H-mode target plasmas. Since these plasmas were at high density where the LH waves do not penetrate into the core plasma, rotation changes are due to modifications in the edge caused by the LH waves. A discussion of results is presented in section VI, and various components of the momentum flux, which can be modified by LH waves, are examined.

II. Velocity Changes during LHCD in Ohmic Target Discharges; Plasma Current and Electron Density Dependence

Shown in Fig.1 are the time histories of several parameters of interest for a 5.4 T, 0.91 MA (q_{95} = 3.7) USN deuterium discharge into which 0.9 MW of LH power ($n_{||}$ = 1.6) were injected between 0.8 and 1.3 s. While there was a modest increase in the electron temperature, the line averaged electron density held constant at $0.7\times10^{20}/m^3$. There was a 10% drop in the internal inductance, l_i, due to the LH power, indicating a broadening of the current density profile, which evolved on a time scale of several hundred msec, of order the current relaxation time ($\sim$150 ms), but in any case substantially longer than the global energy confinement time ($\sim$30 ms). There was also a drop in the loop voltage, a slight rise in q_0 calculated from EFIT [26], and a substantial increase in core hard x-ray emission. Estimated driven current was 0.5 MA out of 0.9 MA based on the loop voltage drop. There were sawtooth oscillations throughout the duration of the LHCD. There was a concomitant change in the core toroidal rotation

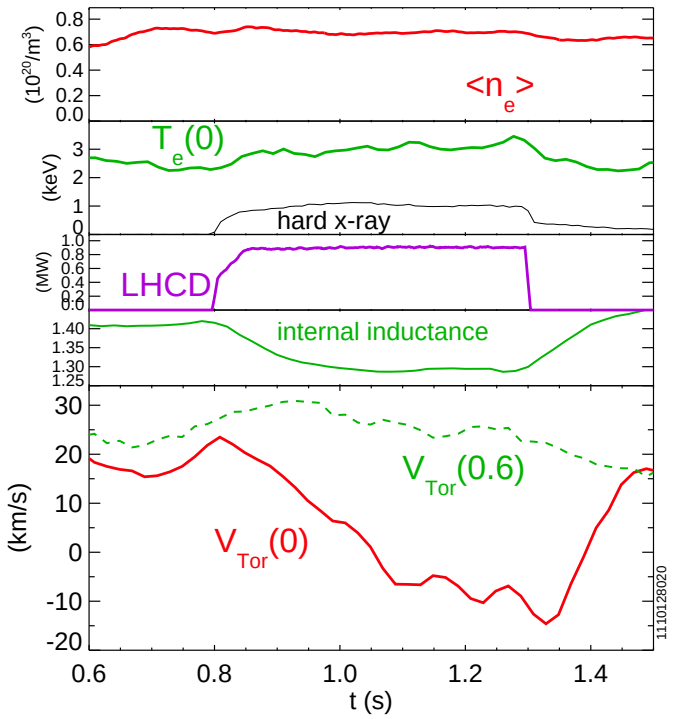

Figure 1: Time histories of the line averaged electron density, central electron temperature (and core hard x-ray emission), LH power, internal inductance and toroidal rotation velocity from He-like Ar along two lines of sight (solid line through the plasma center and dashed line tangent to r/a = 0.6)) for a 5.4 T, 0.91 MA (q_{95} = 3.7) USN discharge.

velocity, incrementing in the counter-current sense from $\sim$+20 km/s (co-current) to ~-10 km/s (counter-current), which also evolved on a time scale of $\sim$200 ms; there was no velocity change outside of the mid radius, confirmed by edge charge exchange measurements. This counter-current trend agrees with the wave momentum input direction and is consistent with previous C-Mod observations [15, 16] at a similar plasma current. Shown for comparison in Fig.2 are the same traces for a 0.42 MA (q_{95} = 7.7) discharge with the same target density and similar LH power. While there was an anal-

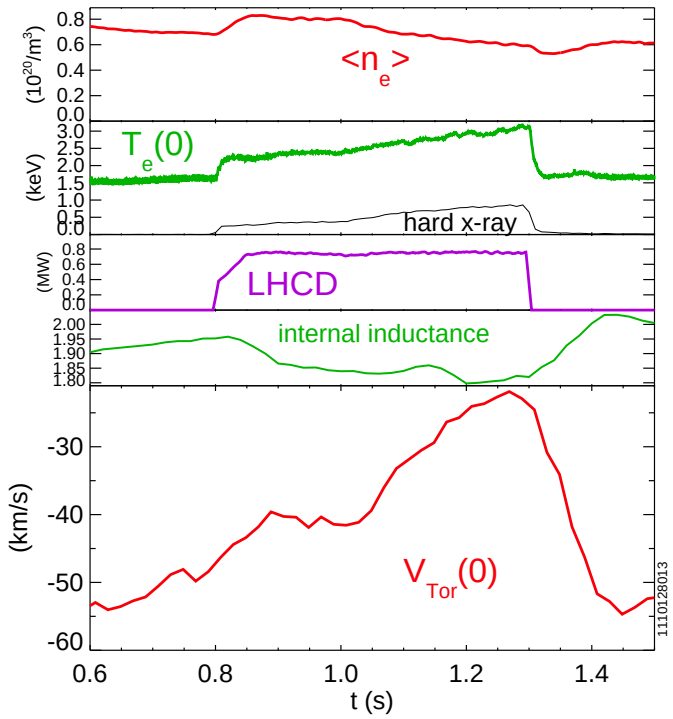

Figure 2: Time histories of the line averaged electron density, central electron temperature (and core hard x-ray emission), LH power, internal inductance and central chord rotation velocity for a 5.4 T, 0.42 MA (q_{95} = 7.7) USN discharge.

ogous evolution of l_i and hard x-ray emission (and drop in the loop voltage) as in the higher current example, in this case the increment in the central chord rotation velocity was in the co-current direction, going from ~-50 km/s before application of the LH power to ~-25 km/s at the end of the LH wave injection. The rotation evolution is more complicated than that observed in Fig.1, perhaps evolving on a faster time scale. Compared to the plasma shown in Fig.1, application of LH power drove a larger fraction of the total plasma current (0.3 MA out of 0.42 MA) and led to a loss of sawteeth at $\sim$0.97 s. This co-current increment of the toroidal rotation with LHCD is similar to

previous observations from JT-60U [12, 14], Tore Supra [13], JET [8] and EAST [17].

It is important to understand what causes this bi-directional rotation with LHCD. This observed bi-directionality seems to rule out direct momentum input, since the waves are launched in the same direction in all cases. Interestingly, the input torque from LH waves [8, 19], $Rn_{\parallel}P_{LH}/c \sim 0.002$ Nm, is similar in magnitude to the torque required to accelerate the core plasma with density $<n_e>$ = 0.7×10^{20}/m^3 by 30 km/s in 0.4 s, about 0.003 Nm. This is a lower limit to the required torque, assuming long momentum confinement. To address this rotation increment direction issue, an examination of rotation characteristics has been performed during a comprehensive plasma current scan. A comparison of the core toroidal rotation velocity evolution following application of LH power for several different plasma currents, at fixed target electron density, in the USN configuration, is shown in Fig.3. The final velocity increment is

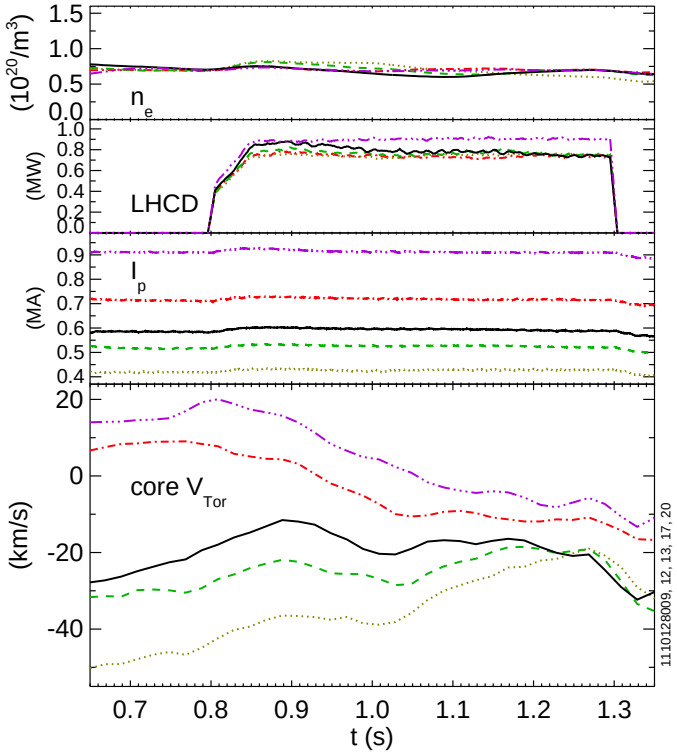

Figure 3: Time evolution comparison of the electron density, LH power, plasma current and core toroidal rotation velocity for five 5.4 T USN discharges with plasma currents of 0.91 MA (dash-dot-dot-dot line), 0.71 MA (dash-dot), 0.58 MA (solid), 0.52 MA (dashed) and 0.42 MA (dotted).

in the counter-current direction for higher target plasma current and in the co-current direction for the lower plasma currents. At the intermediate plasma current (0.58 MA),

there is very little net change in the core rotation, which remains at ~ -15 km/s; this value serves as a velocity asymptote for the higher and lower current cases, at least for this LH input power. A counter-current offset has been observed in DIII-D magnetic braking experiments [38, 39]. The change/increment in the core rotation velocity (the difference in the time averaged velocity at the end of the LH pulse, 1.2-1.3 s, and the pre-LH phase, 0.7-0.8 s) as a function of plasma current, for a series of 5.4 T discharges with $n_e = 0.7 \times 10^{20}/m^3$ and LH power between 0.75 and 0.9 MW, is shown in Fig.4. The *change* in steady state rotation varies strongly with plasma current, go-

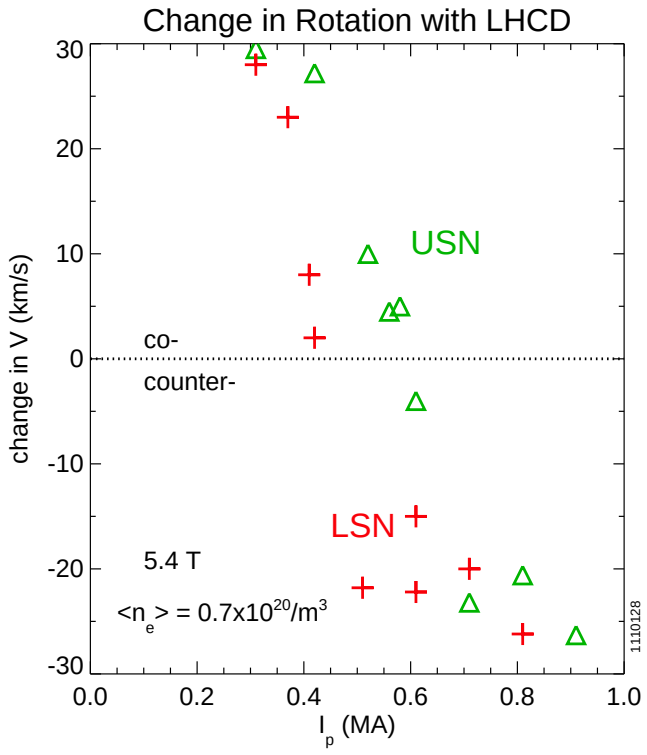

Figure 4: The change in the central chord averaged toroidal rotation velocity during LHCD (0.75-0.9 MW) as a function of plasma current for 5.4 T, USN (triangles) and LSN (plus signs) discharges with $n_e = 0.7 \times 10^{20}/m^3$.

ing from $\sim +30$ km/s at the lowest current (0.32 MA, q_{95}=9.6) to around -25 km/s at the highest current (0.91 MA, q_{95}=3.7). For the USN discharges (a subset of which is shown in Fig.3), there is a stagnation point for $I_P \sim 0.6$ MA (q_{95}=5.5) for these particular target plasma conditions, where application of 0.8 MW of LH power has little effect on the central rotation. For the LSN plasmas, the stagnation point is at a lower plasma current, $\sim$0.45 MA. The zero crossing point for the USN discharges is very close to the intrinsic rotation reversal critical density and current [40, 41, 42], sug-

gesting a possible connexion between this bi-directional rotation change with LHCD and intrinsic Ohmic rotation reversals. The intrinsic rotation velocity of the Ohmic target plasma also depends strongly on the plasma current [43, 8, 42] as shown in Fig.5, from the same current scans, but before the LH wave injection. For the USN plas-

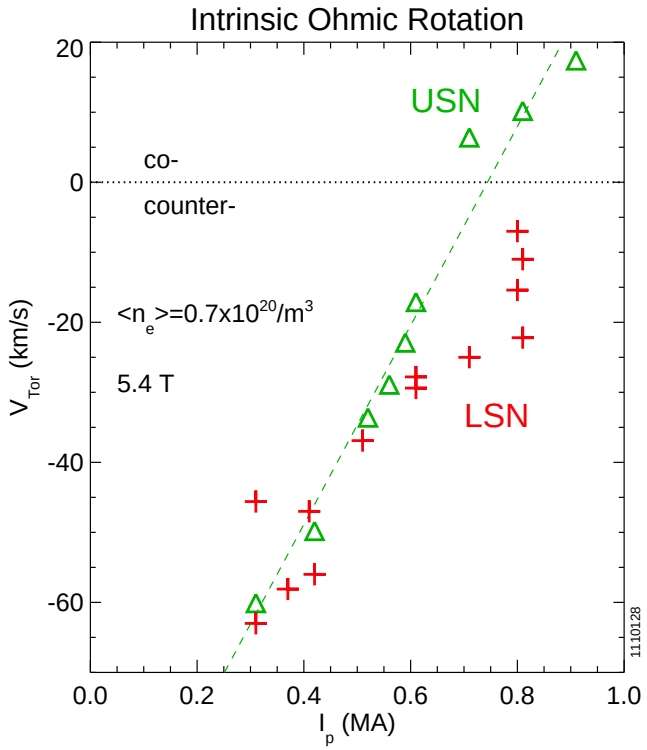

Figure 5: The core toroidal rotation velocity as a function plasma current for 5.4 T, USN (triangles) and LSN (plus signs) discharges with $n_e = 0.7\times10^{20}/m^3$, during the Ohmic phase before LHCD.

mas, the core toroidal rotation varies from -60 km/s at the lowest I_P to $+20$ km/s at the highest, and the intrinsic Ohmic rotation switches direction at $\sim$0.7 MA for this electron density and magnetic field, an example of the rotation reversal phenomenon [43, 44, 45, 46, 47, 40, 41, 42, 48]. The LSN points overlap at the lowest plasma currents, but then diverge as the current is raised above 0.6 MA. For this electron density, the LSN discharges do not exhibit a rotation reversal with increasing plasma current. A comparison of USN and LSN points for 0.8 MA indicates that the core rotation reverses with a change of magnetic configuration [46] due to changes in scrape off layer (SOL) flows [49]. Reversals of intrinsic rotation with changes in the magnetic configuration have been observed in TCV plasmas [50]. It is interesting to note that even though the USN and LSN target plasmas at 0.8 MA were rotating in opposite directions, the

velocity increment with LHCD was counter-current in both cases.

The results of Figs.1-5 documented the core toroidal rotation velocity. Complete velocity profiles for high and low plasma current USN discharges before and during LHCD are shown in Fig.6. For the 0.71 MA Ohmic target plasma, the profile is rela-

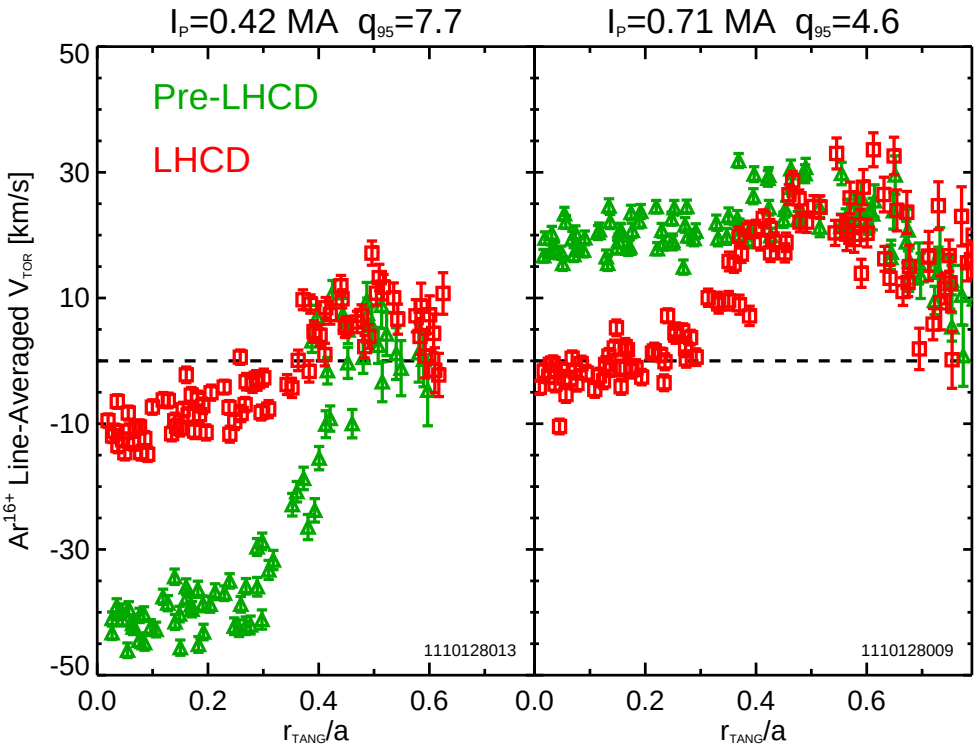

Figure 6: Toroidal rotation spatial profiles before (green) and during (red) LHCD for 0.42 MA (left) and 0.71 MA (right) discharges.

tively flat, with a co-current velocity around +20 km/s across the profile. For the 0.42 MA Ohmic target plasma, the profile is strongly counter-current in the core and has a steep gradient region just inside of the mid radius. During the LH wave injection, the profiles are similar, slightly counter current in the core. These particular shape changes suggest that these profiles are not the result of a momentum pinch effect. There is no change in the profiles outside of the mid radius (r/a$\sim$0.55) with LHCD [15, 16]. This anchoring of the profiles in the vicinity of the mid radius is reminiscent of what is observed during Ohmic rotation reversal [40]. This rotation profile anchoring and the similarity between the LHCD rotation bi-directionality and intrinsic Ohmic rotation reversal critical points suggests that the two phenomena may be related.

III. Comparison to Ohmic Rotation Reversals

The conjecture of a connexion between the Ohmic rotation reversal process and the rotation direction changes in LHCD plasmas will be explored in this section. The intrinsic Ohmic rotation reversal phenomenon is summarized in Fig.7, where the extended operating space with line averaged density and $1/q_{95}$ is shown (combination of USN and LSN discharges). Discharges rotating in the co-current direction are shown

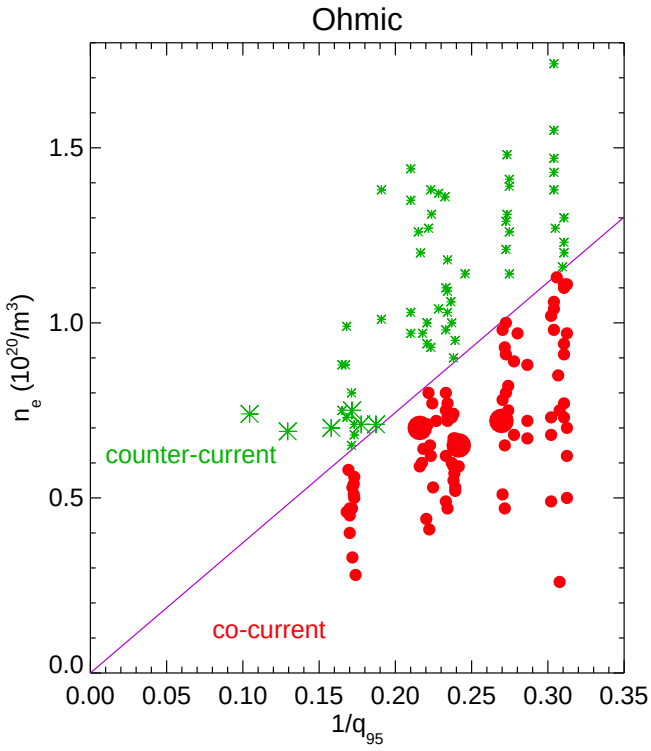

Figure 7: Operational ranges in the n_e-$1/q_{95}$ plane for Ohmic discharges. Dots represent plasmas with co-current rotation while asterisks are for counter-current rotating discharges. The line indicates $n_e q_{95} = 3.7$, with n_e in units of $10^{20}/m^3$.

as dots while those rotating counter-current are depicted as asterisks. There is a very sharp boundary between intrinsic co- and counter- rotating plasmas in the n_e-$1/q_{95}$ plane, which can be parameterized as $n_e q_{95} = 3.7$ [40, 42], the Ohmic rotation reversal condition. The USN points from Fig.5 are shown with the larger symbols.

The cause of this flip in rotation direction is thought to be due to a reversal in sign of the residual stress [51], Π_r, due to a change of domination from trapped electron modes (TEMs) to ion temperature gradient (ITG) modes above a critical collisionality (ν_*) [40, 41, 42]. (Π_r is the component of the momentum flux not proportional to the

velocity or its gradient, whose sign depends on the underlying modes. The divergence of Π_r is the intrinsic tourque density.) This is why the co/counter boundary depends on the product $n_e q_{95} \propto \nu_*$. Π_r also is a function of the gradient of the current density profile [52, 51, 53, 54, 55], and in principle can switch sign through changes in the current density profile by externally driven current *via* LH waves. Related plots for the operational space in LHCD plasmas from selected scans at fixed power are shown in Fig.8, to be compared with Fig.7. Asterisks depict a *change* between the Ohmic target

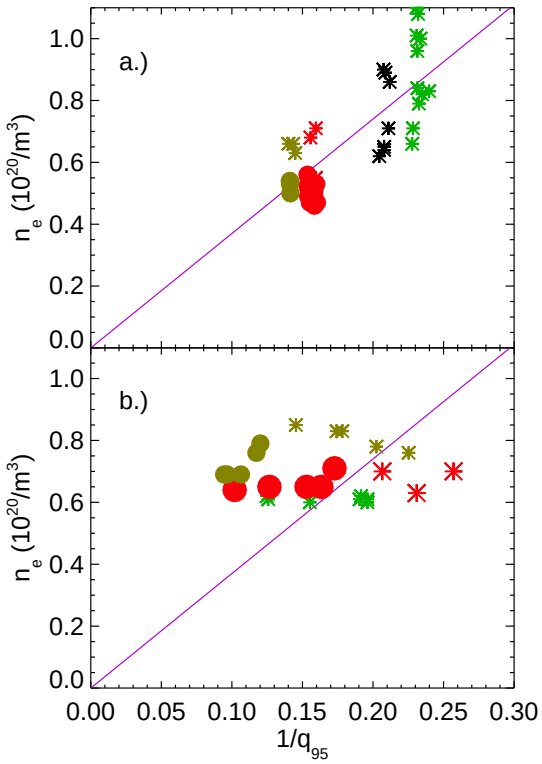

Figure 8: Operating points in the n_e-1/q_{95} plane for LHCD plasmas. Dots indicate an *increment* in the co-current direction with LHCD while asterisks are for *changes* with LHCD in the counter-current direction. In the top frame (a), different shades (colors) are from density scans at fixed current while in the bottom frame (b), current scans at fixed density are shown. The lines indicates $n_e q_{95}$ = 3.7, the Ohmic intrinsic rotation reversal boundary, with n_e in units of 10^{20}/m^3.

and LHCD rotation in the counter-current direction while dots are for *increments* in the co-current direction. The top panel is from dedicated density scans at fixed plasma current while the bottom frame shows the results from current scans at fixed density. The larger points in the bottom frame are from the current scan shown in Fig.4. Different shades/colors are from selected scans. In some scans the switch between co- and

counter-current direction increments with LHCD occurs at the Ohmic rotation reversal critical boundary, while others clearly do not. Also, co- and counter- increments with LHCD appear on both sides of the boundary. Compare the I_P scan points from Fig.4, shown by the larger red symbols in the lower panel, which are for USN plasmas, to the smaller mustard points just slightly above in density, which are for LSN discharges. Since the increment reversal points are different, this suggests that the magnetic configuration can affect the co/counter increment boundary, possibly through the q profile. An up/down asymmetry in shape is also a possibility. It should be emphasized that in the LHCD cases, the symbols represent the *change* in rotation direction, while in the Ohmic examples from Fig.7, the actual rotation direction is shown. A similar plot from the complete LHRF database in L-mode target plasmas, including both USN and LSN plasmas, with power between 0.6 and 0.9 MW, and with $n_{||}$ between 1.6 and 2.5, is shown in Fig.9. It is clear that there is nothing special about the Ohmic rotation reversal

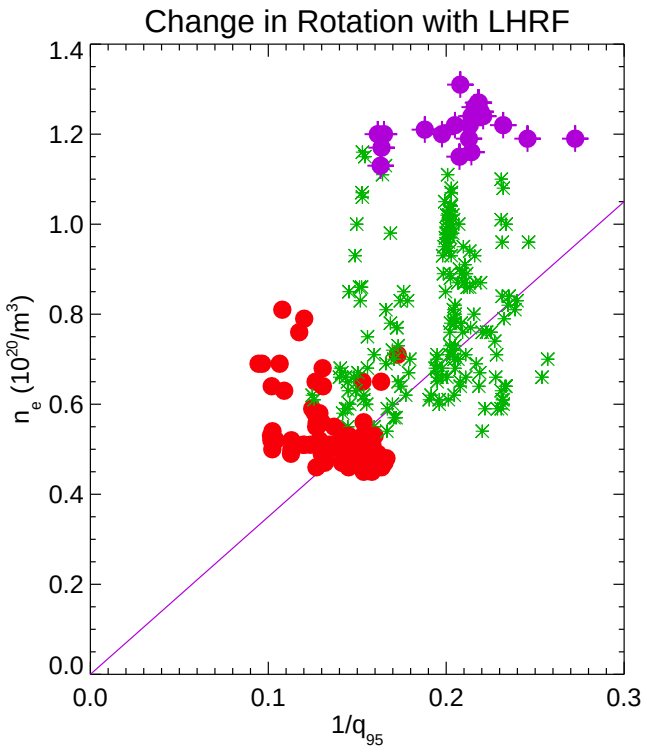

Figure 9: Operating points in the n_e-$1/q_{95}$ plane for L-mode LHRF plasmas. Red dots indicate a *change* in the co-current direction with LHCD while green asterisks are for *changes* with LHCD in the counter-current direction. The purple points (dots with +s) are from high density discharges with poor core LH wave absorption. The line represents $n_e q_{95}$ = 3.7, with n_e in units of $10^{20}/m^3$.

boundary (solid line) and the co/counter rotation *increment* with LHCD. Inspection of this figure indicates that co-current increments with LHCD occur for low density, low current plasmas, which is consistent with the results from JT-60U, Tore Supra, JET and EAST. There is a group of points in Fig.9 (represented by purple dots with '+' signs) indicating a co-current change with LHRF at the highest densities. These discharges, with low core LH wave absorption, will be treated in detail in the next section.

The clustering of LHCD co-current increment points at low density and current suggests that an alternative operational space plot would be more revealing. Shown in Fig.10 is the corresponding graph in the n_e-q_{95} plane for LHCD rotation changes. There is a rough boundary between co- and counter- increments with LHCD, repre-

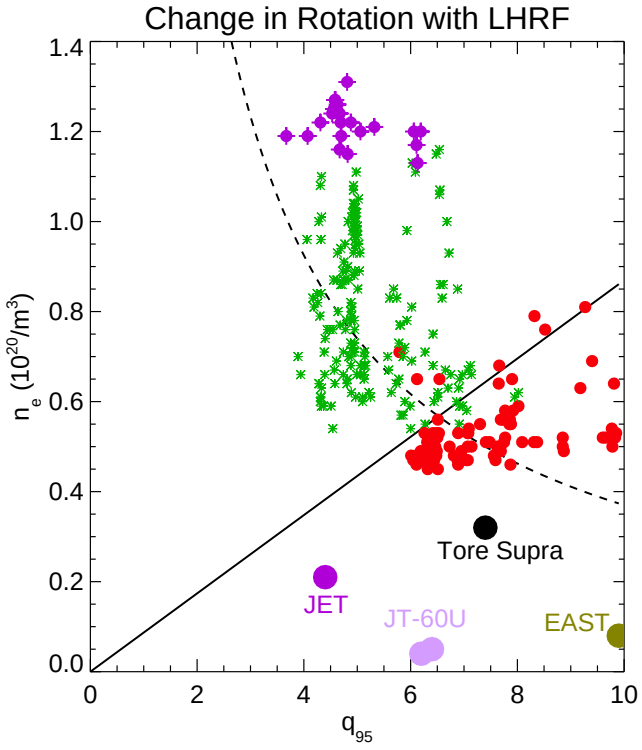

Figure 10: Operating points in the n_e-q_{95} plane for L-mode LHCD plasmas. Dots indicate an *increment* in the co-current direction with LHCD while asterisks are for *changes* with LHCD in the counter-current direction. The solid line represents n_e/q_{95} = 1/11.5, with n_e in units of $10^{20}/m^3$, and the dashed line is the Ohmic rotation reversal boundary, $n_e q_{95}$ = 3.7. Operating points for JT-60U (pink) [12], Tore Supra (black) [13], JET (purple) [8] and EAST (mustard) [17] are also shown.

sented by the line n_e/q_{95} = 1/11.5 = 0.087 (with n_e in units of $10^{20}/m^3$). There is a co-current change in most LHCD plasmas if $n_{e,20} < q_{95}/11.5$. This boundary is not

Device	ΔV	$n_e(10^{20}/m^3)$	q_{95}	n_e/q_{95}	I(MA)	B(T)	R(m)	Ref.
C-Mod	cntr	0.6-1.2	<5	>0.087	0.8	5.4	0.67	[15, 16]
C-Mod	co	0.4-0.6	6-10	<0.087	<0.6	5.4	0.67	[18]
EAST	co	0.08	10	0.008	0.25	2	1.8	[17]
JET	co	0.21	4.4	0.048	2	2.6	2.96	[8]
JT-60U	co	0.05	6.4	0.008	1.2	4	3.4	[12]
JT-60U	co	0.04	6.2	0.006	1.2	3.6	3.4	[14]
Tore Supra	co	0.32	7.4	0.041	0.8	3.7	2.34	[13]

Table 1: Machine and operational parameters for LHCD experiments in L-mode plasmas on various devices. The column marked ΔV indicates whether the change in rotation with LHCD was in the co- or counter-current (cntr) direction.

as precise as the Ohmic reversal boundary (Fig.7) suggesting that there may be other parameter dependences (besides on n_e and q_{95}), such as on the current density profile or the magnetic configuration. For comparison, the Ohmic rotation reversal boundary, $n_e q_{95}$ = 3.7, is shown by the dashed line. (Again, the high density co-current points will be discussed in the next section.) Also shown are operational points from JT-60U, Tore Supra, JET and EAST LHCD plasmas, consistent with the C-Mod results, with co-current rotation at low density and low plasma current. However, it's not clear what the proper normalization for the electron density should be to get the most relevant comparison with observations from other devices. A summary of the LHCD rotation parameters from various tokamaks is shown in Table 1. The first column gives the rotation increment direction following LHCD.

Another way of approaching the comparison between Ohmic rotation reversals and LHRF-induced rotation is to examine the rotation velocity as a function of the product of n_e and q_{95}. The product $n_e q_{95}$ serves as a proxy for the collisionality. The result for a large number of Ohmic plasmas is shown in Fig.11. For $n_e q_{95} < 3.7$, the intrinsic rotation is directed co-current, and abruptly switches to counter-current for $n_e q_{95} > 3.7$ [40, 42]. The ranges for n_e and q_{95} in this plot are from 0.3 to $2.0\times10^{20}/m^3$ and 2.6 to 7.2, respectively, with both USN and LSN. A related figure for LHRF plasmas is shown in Fig.12, where the *change* in rotation velocity is plotted as a function of the $n_e q_{95}$ product. These discharges are sorted by 'favorable' and 'unfavorable' drift. 'Favorable' drift indicates that the ion B$\times\nabla$B drift direction is towards the X-point. There seems to be no clear boundary in this plot, in contrast to the Ohmic cases, which showed organization by collisionality. One thing that stands out from inspection of this figure is that most of the co-current increment discharges are with unfavorable drift (counter-current with favorable drift). However, this dataset may be biased since most of the unfavorable drift points were obtained with low density and high q_{95}, conducive to good current drive fraction, while most of the favorable drift points were from high density and low q_{95} discharges. The edge cryopump was used to obtain the lowest density discharges; since the cryopump is located in the top of the vacuum chamber, it was necessary to run with USN, and hence unfavorable drift with the normal field direction. There seems to be no dependence on reversed field, and those points (shown

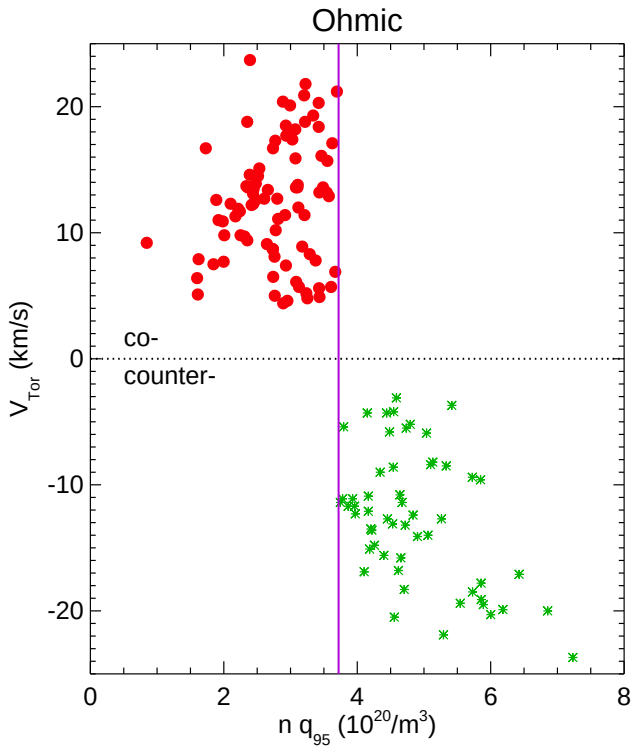

Figure 11: The toroidal rotation velocity as a function of the $n_e q_{95}$ product for Ohmic plasmas. The vertical line is $n_e q_{95}$ = 3.7.

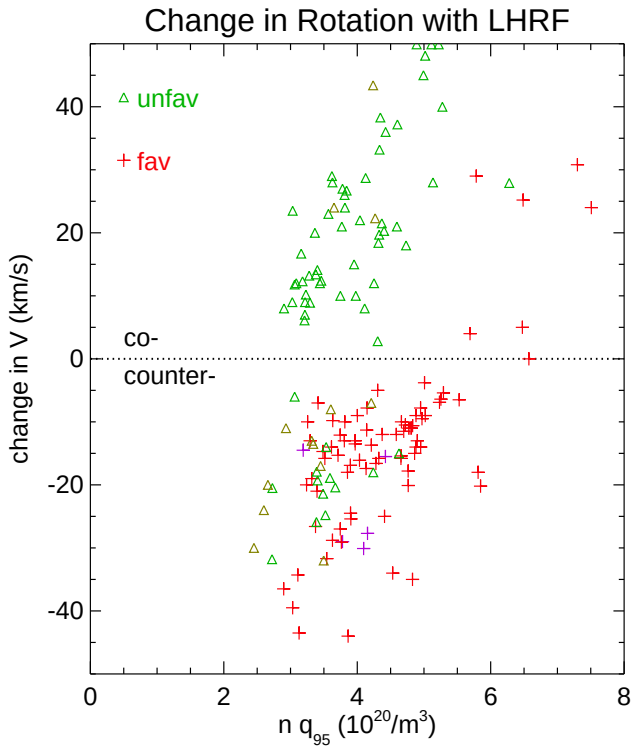

Figure 12: The change in the core toroidal rotation due to LHRF as a function of $n_e q_{95}$. Triangles are for the unfavorable drift while plus signs are for favorable. Lighter shading indicates reversed magnetic field/plasma current.

in lighter shades) are intermixed. It should be noted that when the magnetic field was reversed, the plasma current direction was also reversed. The product $n_e q_{95}$ has the same density and plasma current dependence as the ratio n_e/n_G, where $n_G \equiv I/\pi a^2$ is the density limit in $10^{20}/m^3$, with I in MA and a in m. For the sake of completeness, the data in Fig.12 are shown in Fig.13, where the change in rotation velocity for LHRF plasmas is shown as a function of the n_e/n_G. The scatter is a little larger, but the trends are the same as in Fig.12.

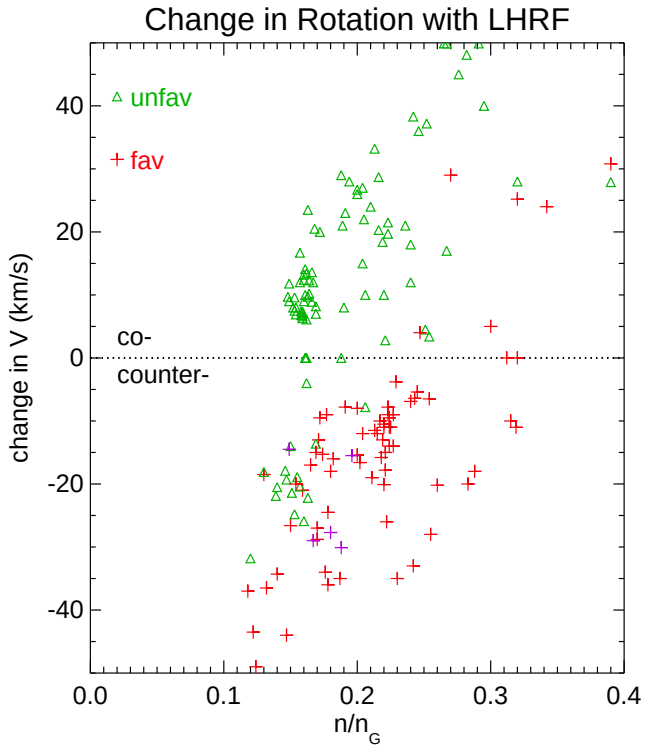

Figure 13: The change in the core toroidal rotation due to LHRF as a function of n_e/n_G. Triangles are for the unfavorable drift while plus signs are for favorable. Lighter shading indicates reversed magnetic field/plasma current.

Application of LH power can give rise to slight perturbations in the electron density, as can be seen in Figs.1 and 2. If the target plasma is very close to the intrinsic Ohmic rotation reversal boundary, this slight change in the density can lead to a reversal (the reversal boundary in Fig.7 is very sharp), which can obscure the effects of LHRF on the rotation. An example is shown in Fig.14, from a 5.4 T, 0.55 MA (q_{95} = 6.0) LSN discharge. Immediately following the LH power injection, there was a 10% increase in the electron density and a drop (and eventual reversal) in the co-current rotation, which evolved on a transport time scale (10s of ms), much faster than the

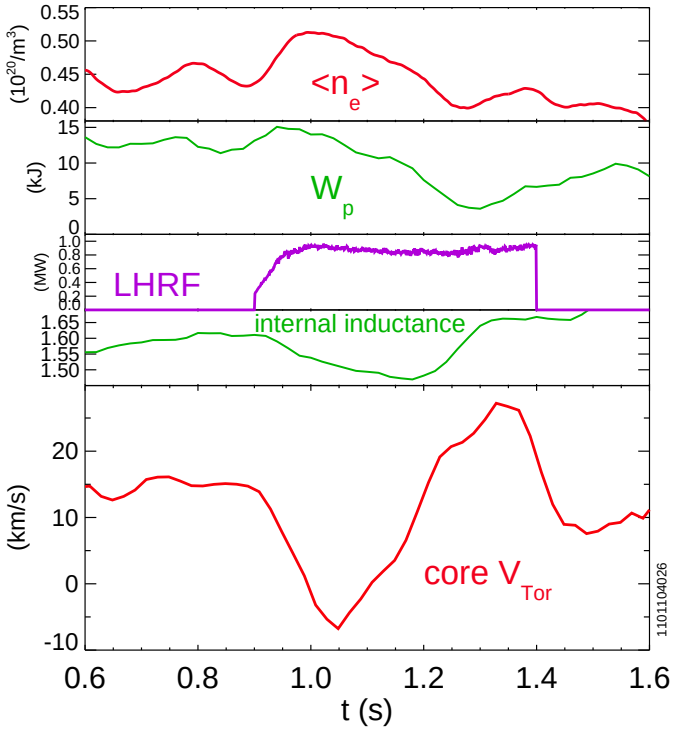

Figure 14: Time histories of the electron density, plasma stored energy, LH power, internal inductance and core rotation velocity for a 5.4 T, 0.55 MA LSN discharge.

velocity changes shown in Figs.1 and 2. After 1.0 s, the density began to decrease and the rotation returned to the co-current direction. This evolution is very similar to the rotation reversals shown in [41]. To complicate matters further, at 1.2 s there was an onset of MHD activity, which led to a drop in the plasma stored energy, an increase in the internal inductance and a loss of current drive. Furthermore, many of these Ohmic L-mode target plasmas, at low density and high current, are close to the threshold for locked mode formation [58, 59]. Locked modes or other deleterious MHD activity can cause a braking of the core toroidal rotation, which in some cases can obscure the effects of LH waves [16]. Discharges with such significant MHD activity, and with complicated velocity evolution (Fig.14), have been excluded in all scaling studies here.

IV. High Density L-mode LHRF Discharges

There was a group of points in Figs.9 and 10 with $n_e \sim 1.2\times10^{20}/m^3$, and low core absorption of the LH waves, which had co-current rotation increments with LHRF power application. The rotation characteristics (evolution and spatial changes) in these discharges also exhibited much different behavior than shown in Section II. Shown in Fig.15 are the parameter time histories of one of these discharges, and two differences immediately stand out. The velocity evolution is on a much shorter than in Fig.1, $\sim$50 ms, close to the energy and momentum confinement times [56, 57] and much shorter than the current relaxation time, $\sim$280 ms. This velocity increase associated with application of LH waves (which have greatly reduced core absorption at this high density [60, 34]), develops on a transport time scale, rather than on a current relaxation time scale. The effect on the rotation is also seen in the outer regions of the plasma (r/a $\sim$ 0.9), which was not observed in Fig.6. There was a slight (4%) drop in the internal inductance during the LHRF injection and a modest increase in the core hard x-ray emission, but very little change in the plasma stored energy or the energy confinement time. The appearance of these LHRF-induced co- rotation L-mode discharges at higher density seems to be independent of q_{95} over the range from 4-6. Shown in Fig.16 is the *difference* of the velocity profiles during and before the LH power pulse. The entire velocity profile during the LHRF injection is elevated in the co-current direction by about 10 km/s compared to the Ohmic intrinsic rotation profile before the LHRF. This is in contrast to the changes shown in Fig.6 where the profiles only varied inside of r/a = 0.5 with LHRF. A possible scenario for this behavior is that absorption of the LH waves in the scrape off layer (SOL) leads to a loss of electrons, which give rise to a positive edge E_r increment, in this case of about 10 kV/m, which drives the co-current rotation throughout the plasma.

V. Velocity Changes with LHRF in H-mode Target Plasmas

LH waves have also been introduced into H-mode target plasmas, with varying levels of core wave penetration. An example is shown in Fig.17, where 0.65 MW of

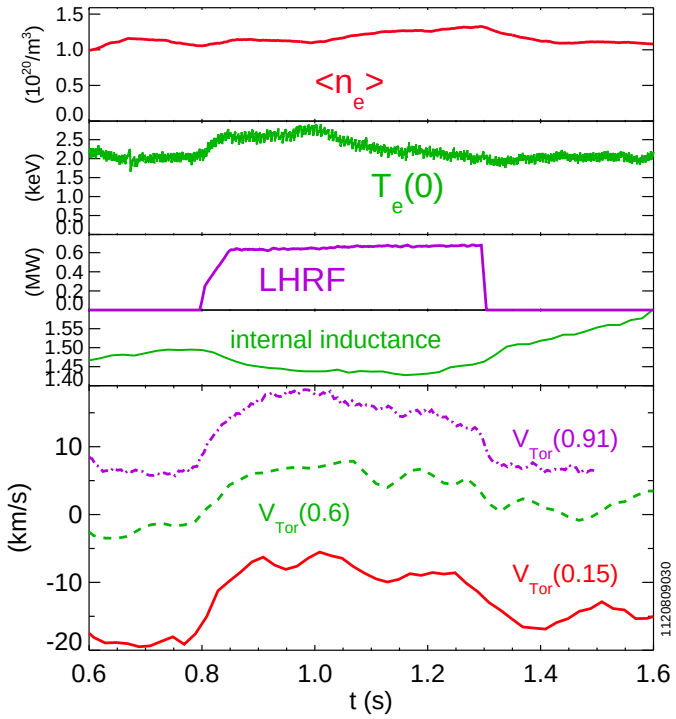

Figure 15: Time histories of the line averaged electron density, central electron temperature, LH power ($n_{||}$ = 1.9), internal inductance and rotation velocity in the core (solid), mid-radius (dashed) and edge (dot-dashed) for a 6.2 T, 0.81 MA (q_{95} = 4.9) USN discharge.

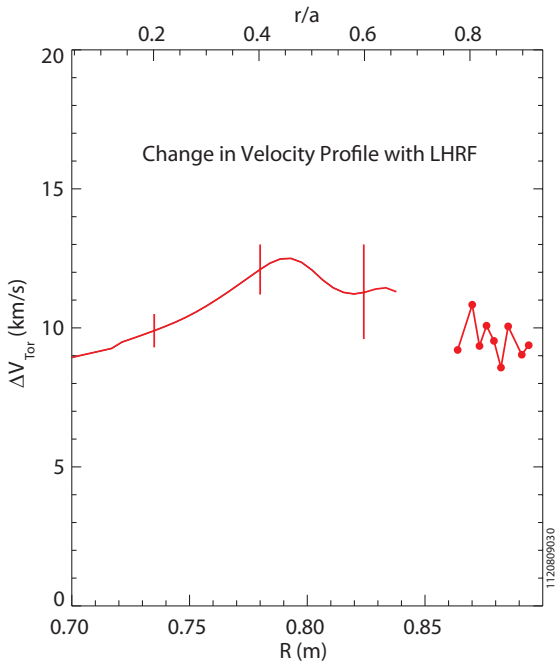

Figure 16: Difference of the radial profiles of the toroidal rotation velocity during and before LH wave injection for the discharge of Fig.15.

LHCD power with $n_{||}$ = 1.9 were injected into a 0.81 MA, 5.4 T (q_{95} = 4.6) LSN H-mode discharge (accessed with 3.6 MW of ICRF minority heating power), with a line averaged density of $3.2\times10^{20}/m^3$. The density at the last closed flux surface (LCFS) was $\sim2\times10^{20}/m^3$, making the LH waves classically inaccessible. Even though at this

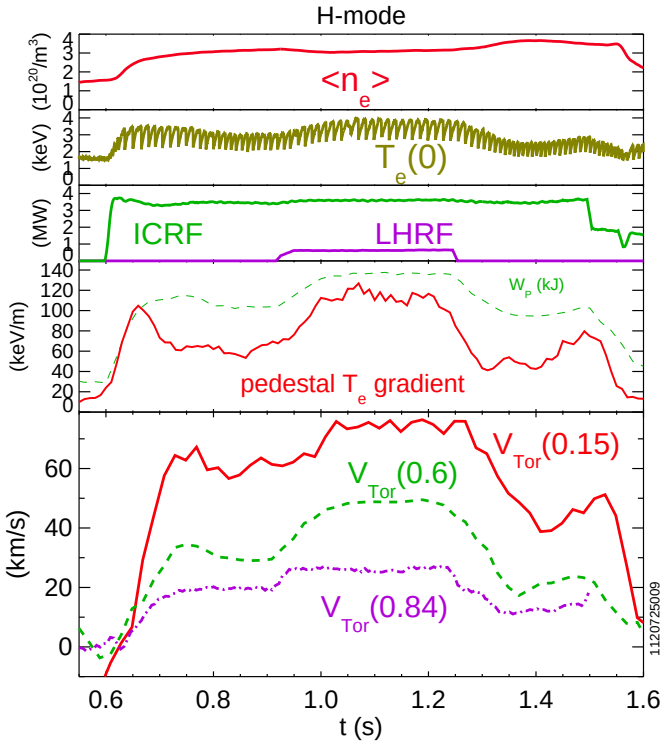

Figure 17: Time histories of the line averaged electron density, central electron temperature, ICRF and LHRF power, pedestal electron temperature gradient and rotation velocity in the core (solid), mid radius (dashed) and edge (dash-dot) for a 5.4 T, 0.81 MA (q_{95} = 4.6) LSN H-mode discharge.

electron density the LH waves have difficulty accessing past the SOL [60], there was a substantial increase in the central electron temperature and a co-current increment of the toroidal rotation at the time of the LHRF power injection. The rotation evolved on a transport time scale ($\sim$40 ms) and the co-current increase was first seen in the plasma periphery. In fact, a co-current increment in the toroidal rotation at r/a = 0.84 appeared immediately after the waves were injected. This suggests that the LH waves affect the properties of the edge plasma, and the changes in rotation are due to subsequent transport effects. There were only slight changes in l_i and the loop voltage during the LH wave injection in this case, and only a very small increase in the core hard x-ray emission.

There was a significant increase in the plasma stored energy and edge pedestal electron temperature gradient (third frame) during the LH wave injection. This increase in the pedestal temperature gradient is mainly due to an increase of the electron temperature at the top of the pedestal. An increase in the edge temperature gradient has been shown to give rise to co-current toroidal rotation in the core [55]. There were also substantial increases in the energy confinement time with LHRF, from 29 to 40 ms, and an increase in H_{98}; all of these changes are consistent with an improvement in edge confinement due to the deposition of power in the edge from the LH waves. From a plasma performance perspective, the additional LH power is quite efficient; for an 18% increase in auxilliary power there was a 28% increase in the plasma stored energy (third frame), a 38% increase in the global energy confinement time and a 32% increase in H_{98}. The cause of such a relatively large effect from such a small amount of additional power is not clear. Indeed LHRF power injection into these high density H-modes does not always show such large confinement improvements, and in some discharges the confinement improvement was lost while the LHRF power was still on. Clues for this behavior may be found from examination of effects observed in the edge region.

In high density H-mode discharges with LHRF power injection, significant changes are observed in the lab frame central frequency of the Quasi Coherent Mode (QCM). This mode exists only in the pedestal/near SOL region on the low field side (LFS), and is responsible for the reduced confinement of particles and impurities in EDA H-mode as compared to ELM-free H-modes [61]. In the lab frame, this mode propagates in the electron diamagnetic drift (EDD) direction with $k_\theta \sim$ 1.5-2 cm^{-1} (at the LFS midplane). Associated with the increase in stored energy obtained with LHRF power injection, the central frequency of this mode is seen to downshift from $\sim$100 kHz to roughly half that frequency, as seen in Fig.18. (This is from a discharge similar to that shown in Fig.17.) Assuming that this is the result of a Doppler shift only (k_θ changes by $<$10%), the change in QCM frequency is consistent with 1.) an incremental co-current increase in toroidal rotation at the QCM radial location of $\Delta V_\phi = \Delta(\omega_0{}^{QCM}/k_\theta{}^{QCM})\ (B_\phi/B_\theta) \sim$ 9 km/s, 2.) an increase of $\sim$7 kV/m in the presumed negative E_r at the QCM location, leading to a $\sim$1.7 km/s decrease in V_{ExB} or 3.) some combination of these. Since a $\sim$5-7 km/s incremental co-current change in V_ϕ is measured spectroscopically in this region (see Fig.19), most of the change in the QCM frequency is likely due to this co-current velocity change. Similar discharges that have little or no confinement improvement with LHRF power injection show no such frequency downshift; when the confinement increment is lost while the power is still on, the QCM central frequency up-shifts to the larger frequency on a 10-20 ms timescale. These results suggest the possibility of using LHRF as a tool to affect plasma rotation and confinement *via* direct modification of quantities at the plasma edge. Note that many prior C-Mod H-modes with LHRF have shown confinement improvements in the absence of a co-current change in edge toroidal rotation [23]. Reasons for these differences are not clear, although there may be significant differences in the quality of LH wave absorption.

The *increment* in the velocity profile, observed after the addition of steady LHRF power to an ICRF only H-mode discharge, is shown in Fig.19. (This is from a discharge similar to that shown in Figs.17 and 18.) For ICRF H-mode plasmas, the toroidal rotation is strongly co-current over the entire core region [57]. Addition of LHRF

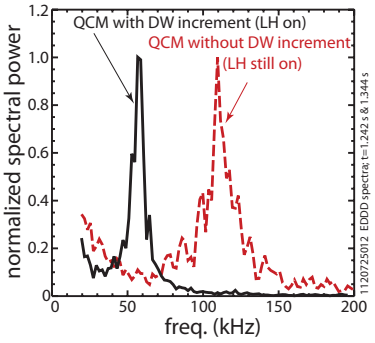

Figure 18: Lab frame frequency changes seen in the QCM, as measured using gas puff imaging. In black is the normalized fluctuation power spectrum during a 5 ms time interval with 0.6 MW of LHRF power injected and a 25-30% increase in stored energy brought about by the LHRF wave injection. The red dashed curve is the spectrum while the LHRF power was still on, but the incremental increase in the stored energy had been lost. The measurements were made just below the outboard midplane and map to a location $\sim$8 mm inside the LCFS.

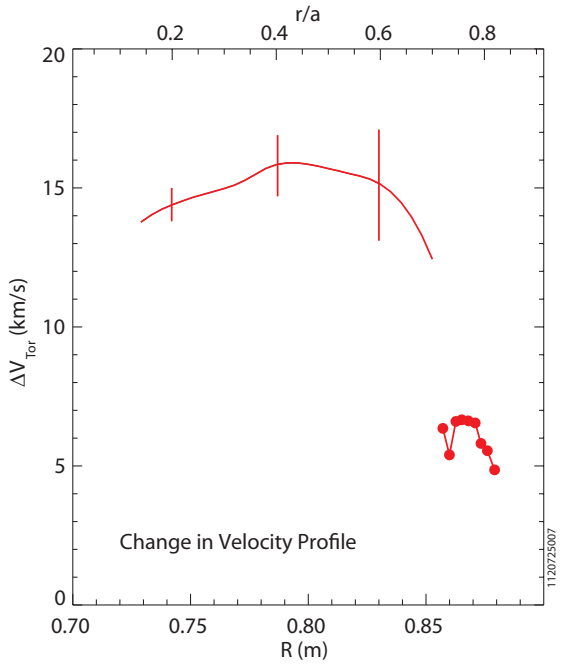

Figure 19: The change of the toroidal rotation velocity profile for a discharge similar to that shown in Fig.17, the difference between the ICRF + LHRF interval and the ICRF only portion.

power to this plasma further increases the core region by about 15 km/s in the co-current direction. The velocity change in the edge region was about a factor of two lower. The likely explanation for this co-current rotation drive is similar to the standard H- and I-mode picture. The additional power gives rise to an enhanced E_r shear, which reduces turbulence leading to an improvement in confinement and a steepening of the edge temperature gradient in the pedestal, which then drives the toroidal rotation *via* the residual stress [55].

Instances of counter-current rotation increments due to LH waves injected into H-mode plasmas have also been observed [16, 23]. These cases may have some degree of wave accessibility inside the LCFS. One such example is shown in Fig.20, which demonstrates the effects of 0.45 MW of LHRF power with $n_{||}$ = 1.9 injected into a 0.62 MA, 5.4 T (q_{95} = 6.3) USN H-mode discharge at a line averaged electron density of $1.6\times10^{20}/m^3$ ($1.4\times10^{20}/m^3$ at the LCFS), accessed with 2.0 MW of ICRF minority heating power. There is a distinct counter-current increment in the core rotation, which

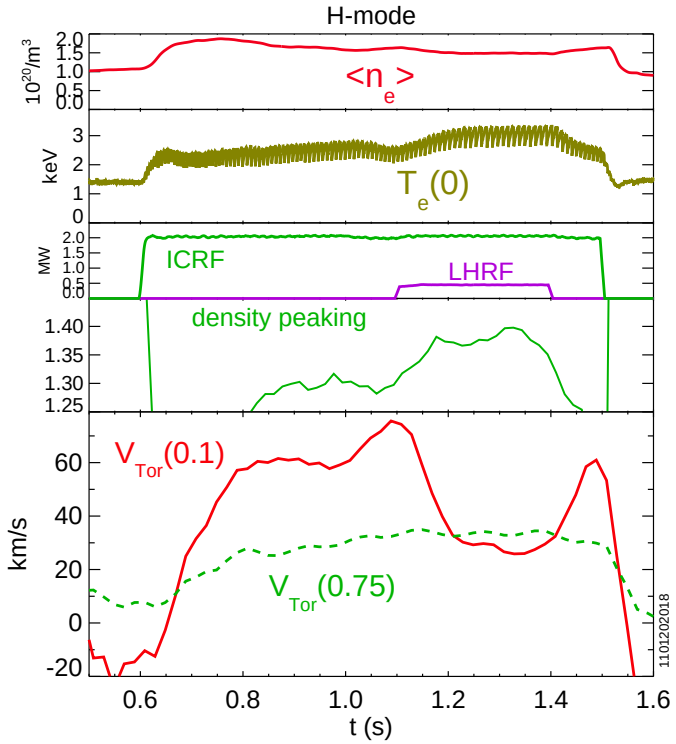

Figure 20: Time histories of the line averaged electron density, central electron temperature, ICRF and LHRF power, electron density peaking (ratio of core to edge) and rotation velocity in the core (solid) and edge (dashed) for a 5.4 T, 0.62 MA (q_{95} = 6.3) USN H-mode discharge.

evolves on a time scale of ∼50 ms, similar to the global energy confinement time for this discharge, ∼34 ms. In contrast to the previous case (Figs.17-19), there was no change in rotation at r/a = 0.8. For this plasma there was no change in the internal inductance, core hard x-ray emission or the loop voltage due to the LH wave injection. The decrease in the core rotation velocity is correlated with a peaking of the electron density profile. While there was an increase in the core electron temperature, there was no peaking of the temperature profile, and no change in the stored energy or energy confinement time. This peaking of the density profile (fourth frame of Fig.20) is the result of an edge density pedestal reduction [23]. A comparison electron density and toroidal rotation profiles during the ICRF H-mode phase, and with additional LHRF power, is shown in Fig.21. In the top frame is shown the ratio of the electron density

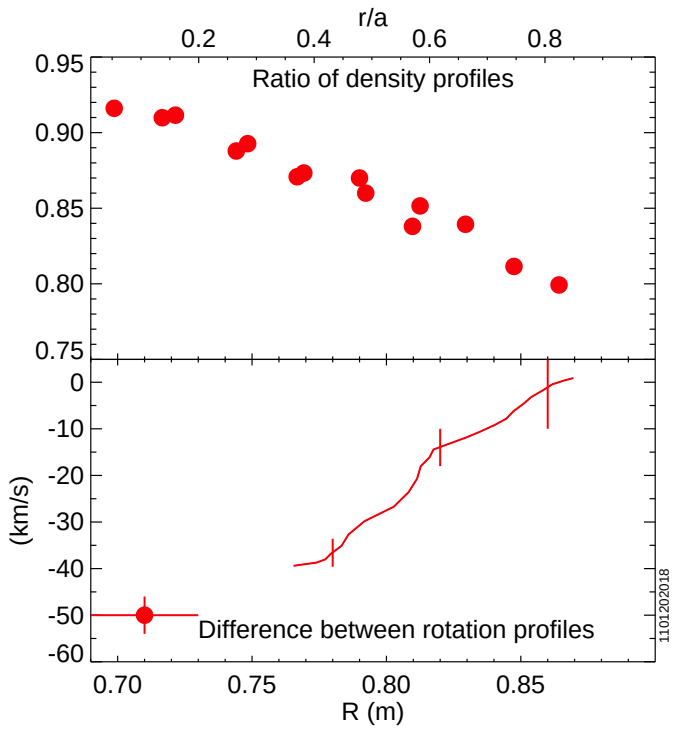

Figure 21: Ratio of the electron density profile with LH waves to the profile with ICRF only (top) for the discharge of Fig.20. In the bottom frame is the change in the toroidal rotation profile, the difference between the profile just before (1.05-1.1 s) and during (1.2-1.4 s) LHRF.

profile during the time interval with LHRF to the profile with ICRF only, and in the bottom frame is the difference in the rotation velocity profile between the ICRF only phase (1.05-1.1 s) and the additional LHRF portion (1.2-1.4 s). The electron density

profile clearly becomes more peaked with the LHRF, while the velocity profile flattens. During the ICRF-only portion of the discharge, the toroidal rotation velocity spatial profile is centrally peaked, which suggests the presence of an inward momentum pinch [56, 57]. With the addition of the LHRF power, the rotation profile becomes flat, which is consistent with a suppression of the inward momentum pinch.

Not all discharges with these H-mode target conditions exhibit the rotation drop or density profile peaking. Shown in Fig.22 is a comparison of two similar ICRF H-mode discharges with additional LHRF power injection (0.93 MW with $n_{||}$ = 2.3). Both 0.61 MA, 5.4 T (q_{95} = 6.6) USN plasmas had a target density of $1.8\times10^{20}/m^3$ during the H-mode phase. The discharge which experienced a decrease in the central rotation

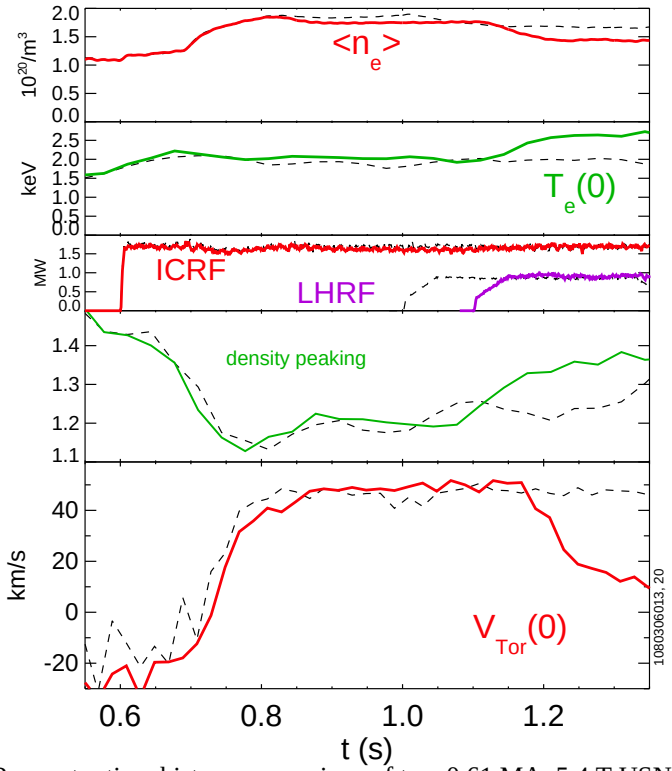

Figure 22: Parameter time history comparison of two 0.61 MA, 5.4 T USN discharges with additional LHRF power. From top to bottom, the line averaged electron density, central electron temperature, ICRF and LHRF power, electron density peaking (ratio of core to edge) and rotation velocity in the core.

with LHRF power showed an increase in the electron temperature and a peaking of the electron density profile. It's not clear what led to this effect in one plasma and not the other, but there is a correlation between a flattening of the velocity profile and a peaking of the electron density profile. One possible difference is that the discharge without the

density peaking and rotation drop had a substantially higher radiated power (by about 25%) at the time of the LHRF pulse, perhaps because this plasma was later in the day, after the boronization wall conditioning had started to wear off. It has been shown [23] that excess core radiation prevents LH-induced modification of the pedestal. The correlation between the counter-current increment in the core rotation (indicative of a flattening of the velocity profile) and the peaking of the electron density profile is demonstrated in Fig.23. The change in the core rotation velocity with LHRF power

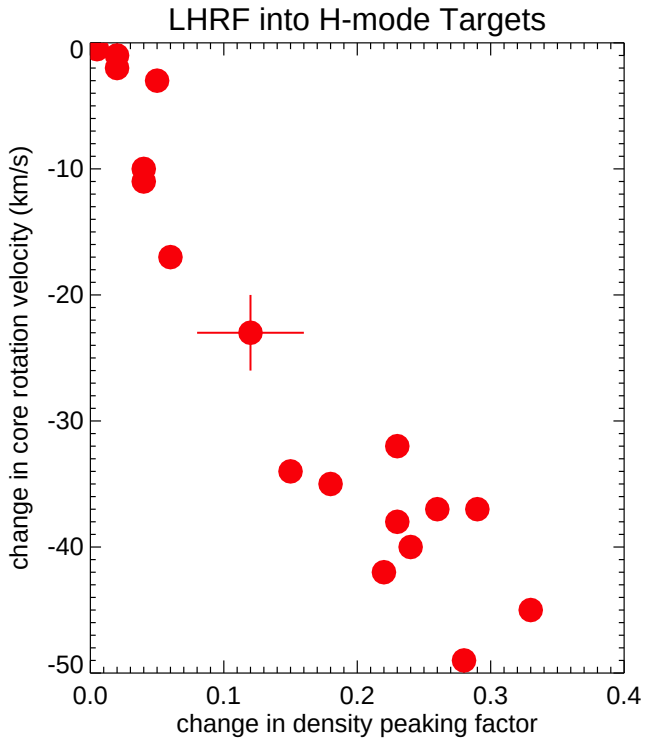

Figure 23: The change in the core rotation velocity as a function of the change in the electron density peaking factor for H-mode discharges with LHRF.

is shown as a function of the electron density peaking factor, here defined as the ratio between the central density and that at the 95% flux surface. There is a strong anti-correlation between the two profile shapes.

For the sake of completeness, two groups of points from H-mode plasmas similar to those shown in Figs.17-23 have been added to the operational space plot in the $n_e - q_{95}$ plane, and are shown in Fig.24. There is a rich variety of LHRF-induced rotation behavior over the C-Mod operating range.

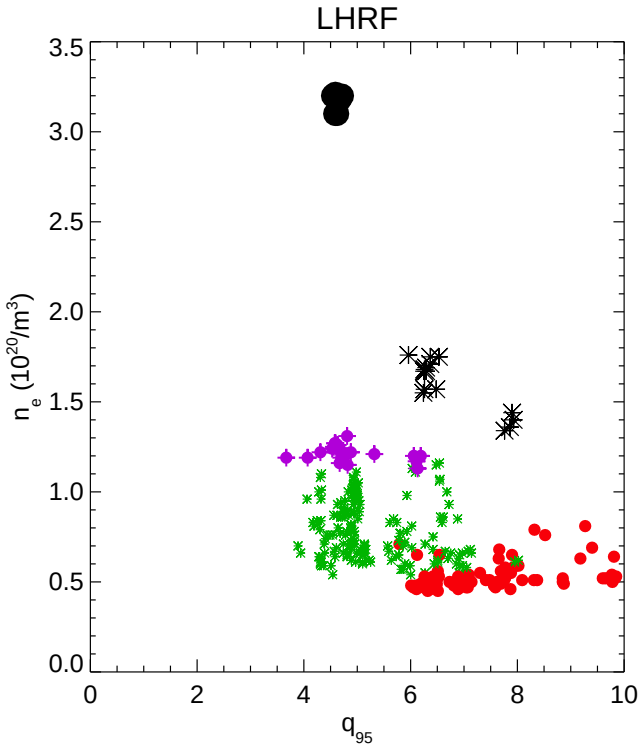

Figure 24: The plot of Fig.10 expanded to include H-mode target plasmas with LHRF. Dots indicate a velocity *increment* in the co-current direction while asterisks are for a counter-current change.

	Fig.1	Fig.2	Fig.15	Fig.17	Fig.20	Fig.22	Fig.22
τ_{V_ϕ} (s)	0.2	$\sim$0.2	0.05	0.04	0.05	0.05	–
τ_{CR} (s)	0.15	0.10	0.28	0.55	0.25	0.26	0.24
τ_{E} (s)	0.03	0.03	0.04	0.04	0.03	0.03	0.03
$\Delta \mathrm{V}_{core}$	cntr	co	co	co	cntr	cntr	n
ΔV profile	core	core	entire	entire	core	core	n
$\Delta \mathrm{V}_{edge}$	n	n	co	co	n	n	n
$\Delta \nabla \mathrm{T}_{ped}$	n	n	n	y	n	n	n
$\Delta \nabla \mathrm{n}_{core}$	n	n	n	n	y	y	n
target q_{95}	3.7	7.7	4.9	4.7	6.3	6.5	6.4
target n_e (10^{20}/m^3)	0.7	0.7	1.2	3.3	1.6	1.8	1.9
core wave abs	y	y	low	n	n	n	n
Δq(r)	low	y	?	n	n	n	n
Δl_i	y	y	low	n	n	n	n
sawteeth	y	n	y	y	y	y	y
hard x-ray	y	y	y	n	n	n	n
drive	e_{pinch}?	∇q	V_{edge}?	$\nabla \mathrm{T}_{ped}$	$\nabla \mathrm{n}_{core}$	$\nabla \mathrm{n}_{core}$	–
momentum flux	source?	Π_r	Π_r	Π_r	V_{pinch}?	V_{pinch}?	–

Table 2: A summary of qualitative changes and parameters for LHRF discharges. 'n' stands for no and 'y' represents yes.

VI. Discussion

The parameters and qualitative changes from the variety of discharges into which LH waves were injected, catalogued in Fig.24, are summarized in Table 2. This compares the relevant time scales, profile shapes, characteristic changes, parameters ranges and drive mechanisms for LHRF plasmas. At the top is given the figure number of a plasma which exemplifies a particular type of response to LHRF injection. The first three rows give the relevant time scales for the core velocity change, current relaxation and energy confinement, respectively. The next three rows indicate the change/increment direction of the rotation velocity and profile. The following rows list other relevant parameter changes and plasma conditions.

There appear to be two general classes of LHRF-induced toroidal rotation changes: those with good core absorption of the LH waves with concomitant current drive and those cases where the LH wave energy is deposited in the periphery. In low density ($<1.1\times10^{20}$/m^3) L-mode target plasmas with good LH wave accessibility and absorption (red and green points in Figs.9, 10 and 24, columns 1 and 2 in Table 2), the core rotation (only inside of r/a$\sim$0.5) evolves on a current relaxation time scale (100s of ms, see row 2). These discharges also have significant changes in the internal inductance and hard x-ray emission. For the lowest density, low current discharges in this class, the rotation change is in the co-current direction, while for higher density, high current plasmas, the rotation increment is counter-current. This may be due to an electron pinch (a direct LH wave effect, more effective with more trapped electrons) or through

	sawteeth	no sawteeth
co-	0	89
counter-	146	8

Table 3: Number of discharges, showing correlation between sawteeth and rotation increment direction with LHCD for low density L-mode target plasmas.

changes in the current density profile, which can change the sign of the residual stress, and hence the rotation direction (discussed below). The counter- increment plasmas (column 1 in Table 2) had sawtooth oscillations, while in the co- increment discharges (column 2), the sawteeth were suppressed due to a significant change in the q profile. Table 3 summarizes the sawtooth behavior for a database of 243 low density target plasmas with LHCD. No co- increment discharges exhibited sawtooth oscillations while all sawtoothing discharges underwent counter-current rotation changes. Only a few counter- increment plasmas were without sawteeth.

In high density target plasmas ($n_e > 1.2\times10^{20}/m^3$), where the LH waves are thought to be damped in the plasma periphery, the rotation across the entire profile evolves on a transport time scale (10s of ms, row 3, Table 2). The influence of the LH waves is indirect, causing changes in the SOL and/or edge plasma, which affect the core plasma, on a transport time scale. (See Table 2 columns 3-7)

Consider first the behavior shown in Figs.15 and 16 (3^{rd} column Table 2), which is arguably the least complex of all of these cases (purple points in Figs.9, 10 and 24). The LH waves, which have poor core absorption at this density [62], are damped in the plasma edge. An increase in the SOL pressure has been observed on edge probes, indicating an edge perturbation. At the same time, there was an increase of the radial electric field, E_r, at r/a = 0.95, from $+20$ kV/m to $+30$ kV/m, associated with changes in the toroidal rotation velocity (see Figs.15 and 16). This increase is consistent in sign with edge electron orbit losses. The co-current toroidal velocity evolves on an L-mode momentum transport time scale [56, 57], a few 10s of ms, similar to the energy confinement time.

The results of Figs.17-19 (4^{th} column Table 2, black dots in Fig.24) are consistent in magnitude and direction with earlier observations of toroidal rotation in ICRF heated H- and I-mode plasmas [55], where the co-current change in rotation has been associated with an increase in the pedestal temperature gradient. A co-current perturbation is first seen at the plasma periphery, and then propagates into the core. This is accompanied by increases in the plasma stored energy and H factor. The important issue is the mechanism by which injection of LH waves (which do not routinely penetrate into the plasma at these high densities) leads to an increase of the pedestal temperature gradient. The underlying concept for the last two cases is that changes to the momentum flux through Π_r, due the LH waves damped in the plasma periphery, lead to an intrinsic torque.

For Figs.20-23 (Table 2 columns 5-7, black asterisks in Fig.24), there is a flattening of the rotation profile which evolves along with a peaking of the electron density profile, suggesting a reduction of inward momentum transport, either due to a reduc-

tion of an inward momentum pinch, or to a modification of Π_r. This is opposite to the predicted trends of the inward turbulent equipartition [63] and Coriolis [64] momentum pinches, which scale as R/L$_n$. Scaling of the momentum pinch with R/L$_n$ is commonly observed [65, 66, 67, 68, 69, 70, 71]. Why this peaking of the density profile (Fig.23) leads to a drop in the momentum pinch, opposite to what is normally seen, is not clear. For the discharge of Fig.20, R/L$_n$ at the mid-radius increased from 2.4 to 3.1 during the LH wave injection, while the velocity profile flattened due to a reduction of the momentum pinch. The peaking of the electron density profile is actually due to a reduction of the pedestal density, with very little change in the central density [23]. The LH waves, which are absorbed in the plasma periphery at these high densities, affect the edge density pedestal, likely through a change in the radial particle transport. In contrast to the two previous cases, changes to the momentum flux could be due to changes in the momentum pinch term.

The examples with good core LHCD power deposition shown in sections II and III (Table 2 columns 1 and 2) will be discussed next, with the goal of explaining the bi-directional rotation changes. A comparison will first be made of discharges at the extremes of the plasma current scan shown in Fig.4. The LHCD wave deposition profiles for two such plasmas (from section II), with currents of 0.32 (q$_{95}$ = 9.6) and 0.91 MA (q$_{95}$ = 3.7), and with $<$n$_e>$ = 0.7$\times$10^{20}/m^3, have been calculated from GENRAY/CQL3D [72, 73], and are shown in Fig.25. LHCD power levels for the two cases were 0.72 and 0.9 MW, respectively. For the 0.32 MA case, the waves are damped closer to the plasma core, and the driven current is estimated to be 0.23 MA, over 2/3 of the total current. For the 0.91 MA discharge, the total driven current is calculated to be 0.5 MA.

Shown in Fig.26 are the electron density and temperature profiles for these same two plasmas, during the LH wave injection. The electron density profiles are nearly identical, while in the high current case, the temperature is considerably higher, and the profile is broader. For both plasmas, Z$_{\rm eff}$ $\sim$ 4. Values for the collisionality, ν_*, at the mid radius are 0.2 (0.91 MA) and 1.3 (0.32 MA), on either side of the linear Ohmic confinement (LOC)/saturated Ohmic confinement (SOC) boundary, determined to be $\nu_* \sim 0.35$ [42, 48]. These two target plasmas are in collisionality regimes dominated by different turbulence types: trapped electron modes (TEMs) for low ν_* and ion temperature gradient (ITG) modes for high ν_*.

Current density profiles have been determined from EFIT calculations constrained by MSE observations [27, 28] enabled by a diagnostic neutral beam [25]. The rotational transform q, magnetic shear ($\hat{s} = r/q\ \partial q/\partial r$) and magnetic shear scale length (L$_s \equiv$ R$_0$q/$\hat{s}$) profiles, for the same two discharges, plus an intermediate current case (0.58 MA), are shown in Fig.27. For the 0.91 MA plasma (which was sawtoothing throughout the LHCD pulse), the q profile (top frame) increases monotonically, with q$_0$ well below 1 at the magnetic axis. The zero crossing at 0.75 m is consistent with the measured sawtooth inversion radius. For the 0.32 MA case, the q profile is flat in the core, with a value just under 2; for the 0.58 MA example, q$_0 \sim$ 1.3. This is consistent with the lack of sawtooth oscillations for these latter two discharges. Another difference between these cases is the magnetic shear (middle frame); for the 0.91 MA plasma, $\hat{s}$ in the core was about 2.5, for the 0.58 MA case $\hat{s}$ was constant near unity, while for the 0.32 MA discharge, $\hat{s}$ was near 0. Interestingly, all three $\hat{s}$ profiles con-

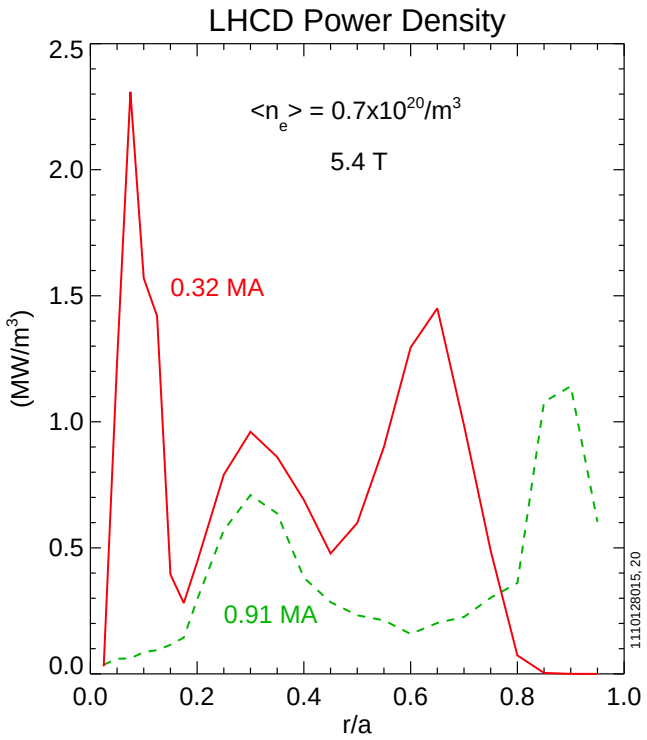

Figure 25: Calculated LHCD power deposition profiles for 0.32 (red solid) and 0.91 (green dashed) MA discharges.

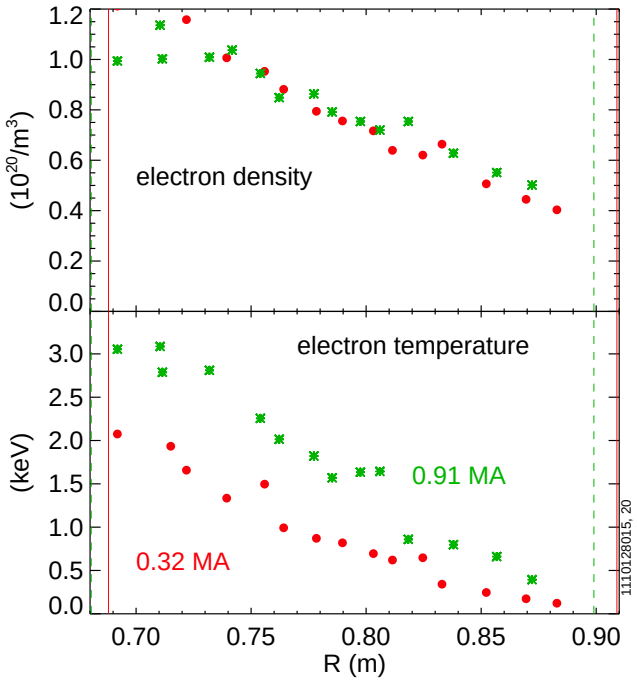

Figure 26: The electron density (top) and temperature (bottom) for 0.91 MA (green asterisks) and 0.32 (red dots) MA discharges with LHCD. Locations of the magnetic axis and LCFS are shown as vertical lines, solid red for the 0.32 MA case and green dashed for 0.91 MA.

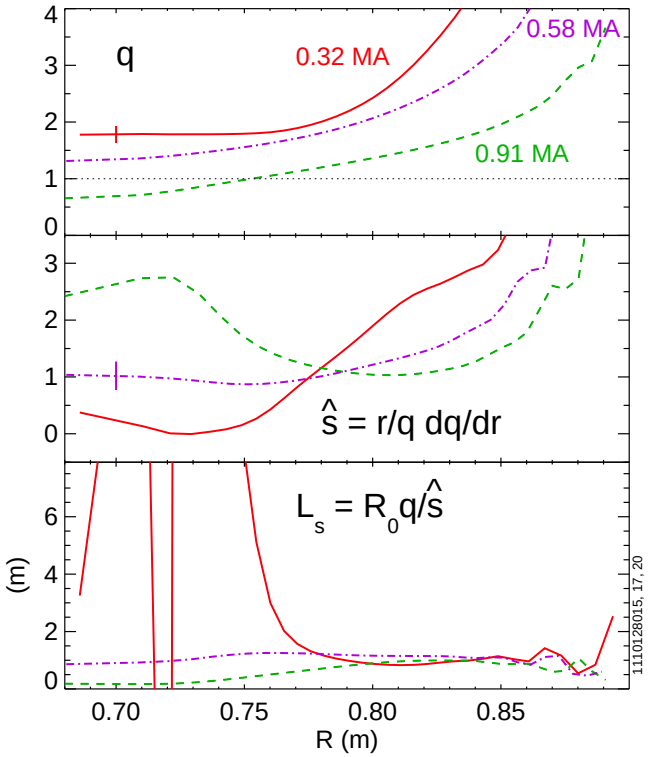

Figure 27: From top to bottom, the rotational transform q, magnetic shear and L_s profiles for 0.32 MA (red solid), 0.58 MA (purple dash-dot) and 0.91 MA (green dashed) discharges with LHCD. Typical error bars are shown.

verge near the mid radius, which is close to the rotation profile stagnation point shown in Fig.6. For the low current case, $\hat{s}$ hovers $\sim$0 which gives rise to an exploding L_s (bottom frame) inside R = 0.75 m (r/a $\sim$ 0.3), exhibiting wildly oscillatory behavior, both negative and positive. For the 0.91 MA plasma, the central L_s was $\sim$ 0.2 m, and $\sim$1 m for the 0.58 MA discharge.

These changes in the q profiles are significant, because the structure of the residual stress, Π_r [52, 53, 54] (which gives rise to an intrinsic torque *via* $\nabla\cdot\Pi_r$), and the turbulent acceleration [74], both depend sensitively on the magnetic shear, $\hat{s}$, and mode structure *via* ion-acoustic coupling. In particular, both drivers of intrinsic rotation require symmetry breaking, so as to set a finite value of $\langle k_\perp k_\parallel |\hat{\Phi}_k|^2\rangle$, necessary for intrinsic torque. Here the bracket refers to a spectral average. To this end, the intrinsic torque can change noticeably [75] as q' and $\hat{s}$ drop, and q'' increases. Furthermore, the intrinsic torque for the normal magnetic shear and 'flat q' cases can differ significantly, although the case may be understated. For weak shear (flat q profiles), non-resonant modes become increasingly important. Recent work [76] has characterized the structure of non-resonant modes and noted that they are best thought of as extended convective cells, with little, if any, similarity to the familiar resonant modes. Further studies [77] have revealed that these non-resonant modes make a substantial contribution to the turbulent heat flux. Thus, there is every reason to expect that the non-resonant modes play an important role in the non-diffusive radial flux of toroidal momentum and the associated Reynolds stress $\langle\tilde{v}_r\tilde{v}_\phi\rangle$. Studies of the effect of non-resonant modes on momentum transport are ongoing and will be discussed in future publications. For now, it should be emphasized that the change in intrinsic torque as LHCD induced current increases and q(r) flattens is quite likely related to the contributions of non-resonant modes. Previous work on turbulence driven intrinsic torque has ignored the effect of non-resonant modes.

The connexion between the magnetic shear and direction of rotation increment is illustrated in Fig.28 where the change in rotation velocity with LHCD is shown as a function of the average value of $\hat{s}$ inside of r/a $\sim$ 0.3. There is an abrupt change in the LHCD rotation increment, going from co- to counter-, near $\hat{s} \sim 1$, exhibiting a sort of threshold behavior. Typical error bars are shown. It should be noted that both USN and LSN points (dots with $\times$) are intermixed, in contrast to the results shown in Fig.4.

A similar threshold is seen as a function of the central rotational transform, as is illustrated in Fig.29, where the change in core rotation frequency is shown depending on q_0. The null in $\Delta\omega$ is close to $q_0 \sim 1$, consistent with the results of Table 3. The use of the rotation frequency allows for direct comparison with the results from other devices; also shown in Fig.29 is a point from EAST [17], which is in qualitative agreement with the C-Mod points.

In order to explore the dependence of LHCD rotation on turbulence, linear gyrokinetic simulations were performed using the gs2 code [78]. These calculations were performed for the 0.71 and 0.42 MA discharges shown in Fig.6, with well characterized rotation increments in the counter- and co-current directions, respectively. Measured electron density and temperature, ion temperature, rotation velocity and q profiles were available for both cases. Linear instabilities were restricted to $k_\theta\rho_i \leq 0.5$, where it was observed that there were common local maxima of the instability spectra. gs2 assumes a Maxwellian electron distribution function, which is not accurate in plasmas with sig-

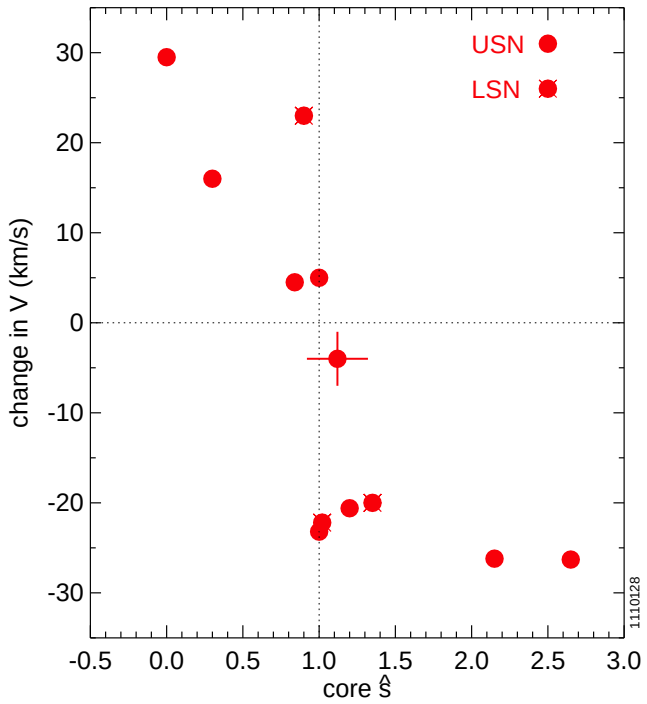

Figure 28: The change in the core rotation velocity with LHCD as a function of the core magnetic shear.

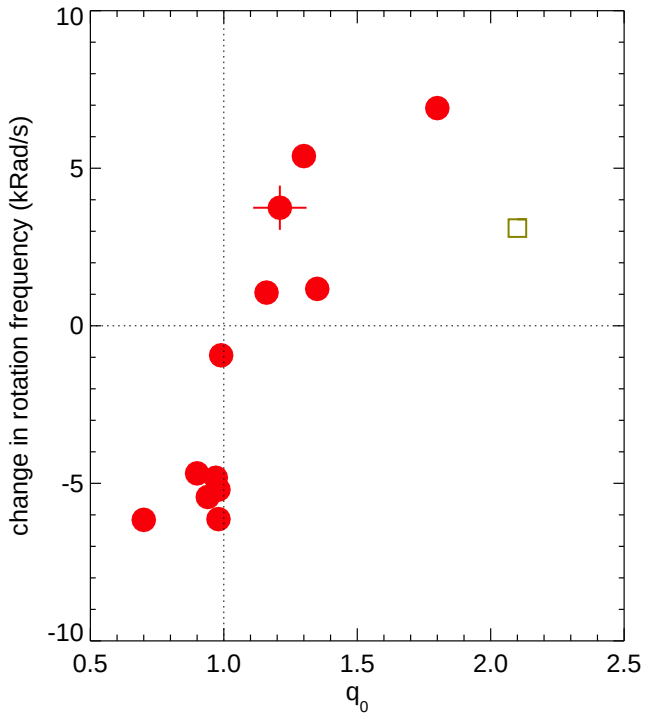

Figure 29: The change in the core rotation frequency with LHCD as a function of q_0. Dots: C-Mod, box: EAST.

nificant LHCD. An estimation of the effect of the non-Maxwellian tail was performed using a high width, low intensity second electron distribution, and it was found that this had a negligible effect on the most unstable linear modes. It was seen that the 0.42 MA discharge had a small section of turbulence propagating in the ion diamagnetic direction, whereas instability propagation in the 0.71 MA case was completely in the electron diamagnetic direction. Overall the mode structure differences between the two cases were not obviously significant. The most unstable mode at r/a ~ 0.5 was selected and sensitivity studies were performed on the most common turbulence driving terms. The two parameters where there were marked differences in the spectra for the two current cases were a/L_n and a/L_{T_i}. For the 0.71 MA discharge, the operational point in a/L_n is very close to the location where the modes switch from the electron to the ion (ITG) direction, which is not observed in the 0.42 MA case. It is expected that the ITG dominated modes, based on arguments of Ohmic rotation reversals, would rotate in the counter-current direction, which is consistent with the LHCD results. For comparison, in the 0.42 MA case, the dependence on density gradient is still strong, but there is no changeover to ion directed modes observed. While this drive mechanism is consistent in these simulations, it does not explain all of the rotation results observed with LHCD. Sub-dominant modes, which are not included, may play an important role and should be included for completeness, and rotation shear may become important in non-linear simulations as well.

The above discussions address the change in sign of the rotation, depending on the q profile, but it remains to account for the original counter-current directed rotation. The simplest explanation is that lower hybrid waves are Landau damped on passing electrons which collisionally transfer the momentum gained from the waves to the ions. The initial torque acting on the ions, as experimentally derived from the rate of change of the ion momentum, is generally consistent with this picture. However more subtle effects may be involved having to do with wave absorption on trapped and circulating electrons, and also the effect of the co-current part of the $k_{\|}$ spectrum. When LH waves interact with trapped electrons in such a way that they would normally have contributed positively to the plasma current, the electrons are instead driven inward to conserve angular momentum [79]. This so-called rf-pinch effect must be quickly ($<$ ms) balanced by an inward ion flow to satisfy the ambipolarity constraint. The resulting Lorentz force acting on the ion flow gives rise to a counter-current torque. At low density and current, the counter current torque due to wave absorption by trapped electrons is usually relatively weak, due to the low fraction of trapped electrons near the core and the high phase velocity of the waves. Passing electrons can also undergo a radial drift due to perpendicular momentum injection and this can lead to either a counter-current or co-current torque depending on whether the parallel index of refraction where the waves are absorbed, $n_{\|abs}$, is less than or greater than n_ϕ, respectively [21]. However, the total torque acting on the ions is that transmitted by the waves radiated by the antenna, namely RPn_ϕ/c, if all effects of frictional momentum transfer and momentum transfer due to the radial drift of passing and trapped electrons are accounted for. The radiated toroidal angular momentum cannot be lost and is fully transferred to ions on the ms time scale.

A challenge to this picture is to explain the change in rotation direction. Any such explanation based only on wave physics is likely to require that the absorbed spec-

trum must be co-directed. In fact, whenever lower hybrid waves are unidirectionally launched so as to accomplish the current drive effect at low $n_{||}$, there is some power launched in the opposite toroidal direction at high $n_{||}$. The power at high $n_{||}$ carries relatively more momentum, by the ratio of the wave number magnitudes; however, the launched power is approximately proportional to $1/n_{||}$ with the result that the momentum carried by waves in the co-current toroidal direction is typically only 20-30% of that launched in the counter-current direction. Nevertheless if the high $n_{||}$ momentum were absorbed, it would contribute to a co-directed torque. Observe, however, that high $n_{||}$ waves have difficulty penetrating the plasma, whereas low $n_{||}$ waves more easily penetrate. In other words, the high $n_{||}$ waves, if absorbed at all, are absorbed peripherally to the low $n_{||}$ waves. Thus, in plasmas where the low $n_{||}$ waves penetrate the plasma core, the high $n_{||}$ waves might be absorbed only in the periphery. Moreover, in plasmas where the low $n_{||}$ waves cannot penetrate the plasma core, but are instead absorbed only in the periphery, the high $n_{||}$ waves might not be absorbed beyond the separatrix, but instead remain in the edge of the plasma within the scape-off layer.

Note also that while there is speculation that the ubiquitous high $n_{||}$ power traveling in the unintended direction might play a role in plasma rotation, this power plays a negligible role in the lower hybrid current drive effect [32]. That is because any momentum put into passing electrons by this part of the spectrum is absorbed by the slower electrons, which quickly share their momentum with the ions, thus extinguishing any current drive role for this part of the spectrum. While quantitatively unlikely in the scenarios described above, it is nevertheless in principle possible for the co-directed waves to dominate the torque balance while the counter directed waves determine the direction of driven current.

There is strong evidence that for the high density ($>1.2\times10^{20}/m^3$) cases shown in Figs.16-23, the changes in the rotation are due to changes in *transport* caused by the LH waves. For low density target plasmas with good core LH wave absorption, the results are consistent with the qualitative explanation. The injected lower hybrid waves carry counter-directed momentum which is Landau absorbed, mainly by passing electrons, and which is transferred by collisions to the ions, resulting in a counter-directed torque. In general, $n_{||abs} > n_{\phi}$, and wave momentum conservation then results in radial flows which lead to a $v_r \times B_{pol}$ toroidal force acting on the ions [21]. The rotation change represents a balance between the applied torque and the effective ion viscosity. However, if the LHCD power level is high enough to drive significant current (to decrease the core $\hat{s}$ or raise q_0 above 1), the sign of the residual stress can change, causing the rotation increment to switch to the co- direction. The last 2 rows in Table 2 summarize the rotation drive agent and appropriate component of the momentum flux. Regardless of the mechanism details, LHRF wave injection may be a powerful tool for both co- and counter- rotation profile control.

VII. Conclusions

In summary, LH waves have been introduced into L- and H-mode target plasmas, resulting in velocity changes in both the co- and counter-current directions. For low

density L-mode plasmas, the rotation direction depends on the resulting changes in the q profile, with co- rotation increments only seen in plasmas with $q_0 > 1$. In these low density cases, the rotation changes are in the plasma core only, inside of r/a = 0.5, and evolve on a time scale similar to the current relaxation time. For high density L-mode target plasmas with poor core LH wave absorption, the rotation changes are in the co-current direction, are seen over the entire profile, evolve on the shorter heat and momentum transport time scales and are caused by edge perturbations. In high density H-mode plasmas, both co- and counter- rotation increments with LHRF are seen. For the co-current rotation increment cases, the edge absorption of LH waves leads to a steepening of the pedestal temperature gradient, which drives co-current rotation in the core, on a transport time scale. For the counter- increment examples, the edge absorption of the LH waves leads to a density pedestal reduction, which steepens the core density gradient, causing a suppression of the momentum pinch, which leads to a flattening of the core velocity profile. These examples exhibit the rich variety of ways that LH waves can lead to changes in the momentum flux.

VIII. Acknowledgements

The authors thank C.Fenzi, F.Nave, M.Yoshida, S.Koide and Y.Shi for information regarding LHCD rotation and the Alcator C-Mod operations, LH and ICRF groups for expert running of the tokamak. Work supported at MIT by DoE Contract No. DE-FC02-99ER54512 and in part by an appointment to the US DOE Fusion Energy Postdoctoral Research Program administered by ORISE.

References

[1] J.E.Rice *et al.*, 2007 *Nucl. Fusion* **47** 1618.

[2] N.J.Fisch, 1987 *Rev. Mod Phys.* **59** 175.

[3] Y.Lin *et al.*, 2008 *Phys. Rev. Lett.* **101** 235002.

[4] Y.Lin *et al.*, 2009 *Phys. Plasmas* **16** 056102.

[5] Y.Lin *et al.*, 2011 *Nucl. Fusion* **51** 063002.

[6] Y.Lin *et al.*, 2012 *Plasma Phys. Contr. Fusion* **54** 074001.

[7] J.-M.Noterdaeme *et al.*, 2003 *Nucl. Fusion* **43** 274.

[8] L.-G.Eriksson *et al.*, 2009 *Plasma Phys. Contr. Fusion* **51** 044008.

[9] J.S.deGrassie *et al.*, 2004 *Phys. Plasmas* **11** 4323.

[10] M.Yoshida *et al.*, 2009 *Phys. Rev. Lett.* **103** 065003.

[11] R.M.McDermott *et al.*, 2011 *Plasma Phys. Control. Fusion* **53** 035007.

[12] Y.Koide *et al.*, in Plasma Physics and Controlled Nuclear Fusion Research 1992 (Proc. 14th Int. Conf. Wurzburg, 1992), IAEA-CN-56/E-3-11, Vol. 1 p. 777, IAEA, Vienna (1993)

[13] P.Platz *et al.*, 22nd European Physical Society Conference on Plasma Physics and Controlled Fusion, Bournemouth, July 1995, Vol. 19C Part III-337.

[14] Y.Sakamoto *et al.*, 2006 *Plasma Phys. Control. Fusion* **48** A63.

[15] A.Ince-Cushman *et al.*, 2009 *Phys. Rev. Lett.* **102** 035002.

[16] J.E.Rice *et al.*, 2009 *Nucl. Fusion* **49** 025004.

[17] Yuejiang Shi *et al.*, 2011 *Phys. Rev. Lett.* **106** 235001.

[18] Y.A.Podpaly, 2012 'Rotation Generation and Transport in Tokamak Plasmas' Ph.D. thesis, Massachusetts Institute of Technology

[19] J.Lee *et al.*, 2011 Proceedings of the 19th Topical Conf. on Radio Frequency Power in Plasmas vol **1406** 459.

[20] Z.Gao *et al.*, 2011 *Phys. Plasmas* **18** 082507.

[21] J.Lee *et al.*, 2012 *Plasma Phys. Control. Fusion* **54** 125005.

[22] Xiaoyin Guan *et al.*, 2013 *Phys. Plasmas* **20** 022502.

[23] J.W.Hughes *et al.*, 2010 *Nucl. Fusion* **50** 064001.

[24] E.S.Marmar *et al.*, 2007 *Fusion Sci. Technol.* **51** 261.

[25] N.P.Basse *et al.*, 2007 *Fusion Sci. Technol.* **51** 476.

[26] L.L.Lao *et al.*, 1985 *Nucl. Fusion* **25** 1611.

[27] J.Ko *et al.*, 2010 *Rev. Sci. Instrum.* **81** 033505.

[28] S.Shiraiwa *et al.*, 2011 *Phys. Plasmas* **18** 080705.

[29] A.Ince-Cushman *et al.*, 2008 *Rev. Sci. Instrum.* **79** 10E302.

[30] M.L.Reinke *et al.*, 2012 *Rev. Sci. Instrum.* **83** 113504.

[31] P.T.Bonoli *et al.*, 2007 *Fusion Sci. Technol.* **51** 401.

[32] N.J.Fisch, 1978 *Phys. Rev. Lett.* **41** 873.

[33] A.E.Schmidt *et al.*, 2011 *Phys. Plasmas* **18** 056122.

[34] G.M.Wallace *et al.*, 2012 *Phys. Plasmas* **19** 062505.

[35] S.G.Baek *et al.*, 2013 *Plasma Phys. Control. Fusion* **55** xxxxx.

[36] G.M.Wallace et al, IAEA proceedings, 2012. Submitted to Nuclear Fusion (2012)

[37] S.Shiraiwa et al, IAEA proceedings, 2012. Submitted to Nuclear Fusion (2012)

[38] A.M.Garofalo *et al.*, 2008 *Phys. Rev. Lett.* **101** 195005.

[39] W.M.Solomon *et al.*, 2009 *Nucl. Fusion* **49** 085005.

[40] J.E.Rice *et al.*, 2011 *Nucl. Fusion* **51** 083005.

[41] J.E.Rice *et al.*, 2011 *Phys. Rev. Lett.* **107** 265001.

[42] J.E.Rice *et al.*, 2012 *Phys. Plasmas* **19** 056106.

[43] J.E.Rice *et al.*, 2005 *Nucl. Fusion* **45** 251.

[44] A.Bortolon *et al.*, 2006 *Phys. Rev. Lett.* **97** 235003.

[45] B.P.Duval *et al.*, 2007 *Plasma Phys. Contr. Fusion* **49** B195.

[46] J.E.Rice *et al.*, 2008 *Plasma Phys. Contr. Fusion* **50** 124042.

[47] B.P.Duval *et al.*, 2008 *Phys. Plasmas* **15** 056113.

[48] J.E.Rice *et al.*, 2013 *Nucl. Fusion* **53** 033004.

[49] B.LaBombard *et al.*, 2004 *Nucl. Fusion* **44** 1047.

[50] Y.Camenen *et al.*, 2010 *Plasma Phys. Control. Fusion* **52** 124037.

[51] P.H.Diamond *et al.*, 2009 *Nucl. Fusion* **49** 045002.

[52] Ö.D.Gürcan *et al.*, 2007 *Phys. Plasmas* **14** 042306.

[53] Y.Kosuga *et al.*, 2010 *Phys. Plasmas* **17** 102313.

[54] Ö.D.Gürcan *et al.*, 2010 *Phys. Plasmas* **17** 112309.

[55] J.E.Rice *et al.*, 2011 *Phys. Rev. Lett.* **106** 215001.

[56] W.D.Lee *et al.*, 2003 *Phys. Rev. Lett.* **91** 205003.

[57] J.E.Rice *et al.*, 2004 *Nucl. Fusion* **44** 379.

[58] R.J.Buttery *et al.*, 1999 *Nucl. Fusion* **39** 1827.

[59] S.Wolfe *et al.*, 2005 *Phys. Plasmas* **12** 056110.

[60] V.E.Golant, 1972 *Soviet Physics Technical Physics* **16** 1980.

[61] M.Greenwald *et al.*, 2007 *Fusion Sci. Technol.* **51** 266.

[62] C.Lau *et al.*, 2012 *Rev. Sci. Instrum.* **83** 10E309.

[63] T.S.Hahm *et al.*, 2007 *Phys. Plasmas* **14** 072302.

[64] A.Peeters *et al.*, 2007 *Phys. Rev. Lett.* **98** 265003.

[65] W.M.Solomon *et al.*, 2009 *Nucl. Fusion* **49** 085005.

[66] M.Yoshida *et al.*, 2009 *Nucl. Fusion* **49** 115028.

[67] P.C.deVries *et al.*, 2010 *Plasma Phys. Control. Fusion* **52** 065004.

[68] T.Tala *et al.*, 2011 *Nucl. Fusion* **51** 123002.

[69] R.M.McDermott *et al.*, 2011 *Plasma Phys. Control. Fusion* **53** 124013.

[70] C.Angioni *et al.*, 2011 *Phys. Rev. Lett.* **107** 215003.

[71] H.Weisen *et al.*, 2012 *Nucl. Fusion* **52** 042001.

[72] A.P.Smirnov and R.Harvey, 1995 *Bull. Am. Phys. Soc.* **40** 1837.

[73] R.W.Harvey and M.McCoy, 1992 in Proc. of the IAEA TCM on Simulation and Modeling of Thermonuclear Plasmas, Montreal, 489.

[74] L.Wang and P.H.Diamond, 2013, 'Gryokinetic theory of turbulent acceleration of parallel rotation in tokamak plasmas', submitted to *Phys. Rev. Lett.*

[75] J.M.Kwon *et al.*, 2012 *Nucl. Fusion* **52** 013004.

[76] S.Yi *et al.*, 2012 *Phys. Plasmas* **19** 112506.

[77] S.Yi *et al.*, 2013, submitted to *Nucl. Fusion*

[78] M.Kotschenreuther *et al.*, 1995 *Comput. Phys. Commun.* **88** 128.

[79] N.J.Fisch and C.F.F.Karney, 1981 *Phys. Fluids* **24** 27.